Vidicon Observations of Mars: Images of the October, 1973 Dust Storm and Two-Dimensional Narrow-Band Photometry

by

Gary Lassiter Johnson

Submitted in Partial Fulfillment
of the Requirements for the
Degree of Master of Science
at the
MASSACHUSETTS INSTITUTE OF TECHNOLOGY
September, 1975

Signature of Author. . . . .
Department of Earth and Planetary Sciences, June 27, 1975

Certified by . . . .
Thesis Supervisor

Accepted by. . . . .
Chairman, Departmental Committee on Graduate Students

Vidicon Observations of Mars: Images of the October, 1973 Dust Storm and Two-Dimensional, Narrow-Band Photometry

by

Gary Lassiter Johnson

ABSTRACT

The major Martian dust storm of October, 1973 was imaged through twenty filters spanning the spectral region from 0.35 microns to 1.03 microns using a silicon vidicon tube. A total of 100 images were taken, each with a resolution of about 200 kilometers. Photographs of vidicon images are presented to show storm phenomena revealed during the 4 hour observation period. Martian short term events are pronounced in the blue, suggesting the presence of dissipating volatiles. Images in the red show the main body of the storm as a dense dust cloud over Solis Lacus. Possible evidence of sudden dust cloud growth in the Aonis Sinus region is discussed. Projected area calculations detect no observable expansion rate in the Solis Lacus cloud during the four hour imaging period. To assess any gross morphological changes in the total srorm system, pictures of artificially rotated images are displayed, each with the storm center mapped to the sub-earth point. Procedures for obtaining from the vidicon images reflection spectra of selected areas on Mars have been developed. Relative reflectance spectra from vidicon images are presented for comparison with relative reflectance spectra from photometer data taken during 3 later nights. Similarities and discrepancies between these data are examined with particular reference to (1) problems imposed by the expanding dust storm and (2) weaknesses in the reduction of the vidicon data. Further data processing of the vidicon images is discussed.

Thesis Advisor: Thomas B. McCord

Title: Associate Professor of Planetary Physics

Acknowledgements

For a year and a half I have been working on the 1973 Mars vidicon data and I would never have gotten this far this fast had it not been for the help and assistance of the people I would like to thank. Carle Pieters provided me with my introduction to vidicon image processing and ever since she has been a source of valuable advise. Bob Huguenin has been a fund of ideas about the realities of the Martian world and has offered helpful guidance during the reduction of the vidicon data. Doug Mink is responsible for the remarkable mapping programs which have supplied this thesis with maps, adding a color and clarity almost justifying all the late nights he spent pouring over the computer's scrawl. Paul Kinnucan and George Fawcett were invaluable during the desperate attempts to debug the programs described in this thesis. Mike Gaffey has been an eminent, unsolicited provider of sundry entertainments. And last but not least, I have Tom McCord to thank for all the successes and rewards I have discovered in the past year and a half for it was he who offered me this project in the first place and supported me thereafter.

Table of Contents

List of Figures

List of Figures

List of Tables

I. Introduction

The mysteries of Mars have been a prolonged and gratifying fascination. In recent years great nations have been provoked into assembling and launching on hazardous voyages spacecraft bound for Mars. The close-up pictures returned to date reveal an evolved and sculptured surface. Although these venturesome craft have unveiled the unexpected, the composition of the Martian soil has yet to be probed in situ.

Remote sensing at telescopic sites on the Earth still provides the most useful method for determining planetary surface compositions. The reflected light of a distant object such as Mars is a nightly signature of the minerals that make up its soil. In the past decade the reflectance spectra of Mars has been studied with increasing success. A surface material of the hydrated iron oxide, limonite, was postulated by Sagan et al (1965) based on similarities observed between the absorption bands in limonite and the albedo curves of Mars determined by Dollfus (1961). With data from the 1967 Mars opposition, Adams and McCord (1969) noted that bright and dark regions on Mars have differing geometric albedos. The surface composition was assumed to be a mixture of oxidized basalts and hydrated iron oxides - dissimilar albedos being indicative of different degrees of oxidation in the same basic material.

During the 1969 opposition McCord and Westphal (1971) using narrow-band photometry detected apparent compositional differences amoung the seven bright and dark areas studied. At the next opposition in 1971, Mariner 9 returned voluminous data. The images from Martian orbit revealed several large scale (far above the Earth-based resolution limit of about 200 km.) geologic terrain types, see Carr et al (1973). Unraveling the subtle compositional differences between regions of differing albedos and terrain types will require a large sample of reflectance spectra from areas which, in some cases, are as small as the resolution limit on Mars. There are, however, important observational difficulties in obtaining this desired photometric data.

Photometry of restricted areas on distant objects involves using a photometer with a very small aperture (about 1mm.). While data is being recorded the aperture must be maintained over the region of study by precision guiding. Problems of drift are unavoidable and the actual area from which data is returned tends to be larger than desired. Very small points of interest as well as regions that are contrast obscured are, therefore, difficult areas to observe photometricly. This is true of such significant features on Mars as the volcanos of Tharsis and the Coprates canyons. Furthermore, rapidly changing events do not lend themselves well to photometric coverage using the photometer/aperture system. If the transient feature is small, such as a local cloud on Mars, the guiding problem becomes significant. On the other hand, if the temporary event is large scale, such as the 1973 Mars dust storm, the photometer cannot study the entire feature in detail and important events may be missed altogether. The solution to these shortcomings is narrow-band photometric coverage of the full disk of Mars. The Vidicon Imaging System has been constructed for this purpose. The intent of this thesis is to describe the photometric value of this versitile imaging system by analyzing the vidicon images of Mars taken during the opposition of 1973.

II. The Vidicon Imaging System

The silicon vidicon imaging system has been developed at the M.I.T. Remote Sensing Laboratory to do two-dimensional precision photometry and low resolution spectroscopy (*). The heart of the system is a RCA silicon diode array vidicon tube. The broad spectral response and high quantum efficiency of the vidicon tube, plus its intrinsic ruggedness and simplicity, provide the astronomer with images better formatted for data reduction than the photographic plate and of comparable spacial resolution. The photometric quality of the vidicon tube has been demonstrated to within 1% of photometer data by Pieters and McCord (1974) and McCord, Pieters and Fierberg (1975).

Photometric images are exposed by opening the shutter and passing the light from the telescope through a filter and onto the silicon diode array (Figure 1). Photons, striking the approximately 1000 by 1000 array of photosensitive diodes, are converted to charge carriers, which discharge the reverse biased diodes. When the shutter is closed an electron beam scans the diode array and recharges clusters of 4 diodes at a time (permitting less precision in the positioning of the electron beam). The resulting current is proportional to the

(*) McCord and Westphal (1972)
McCord and Bosel (1973)
Mink (1974)

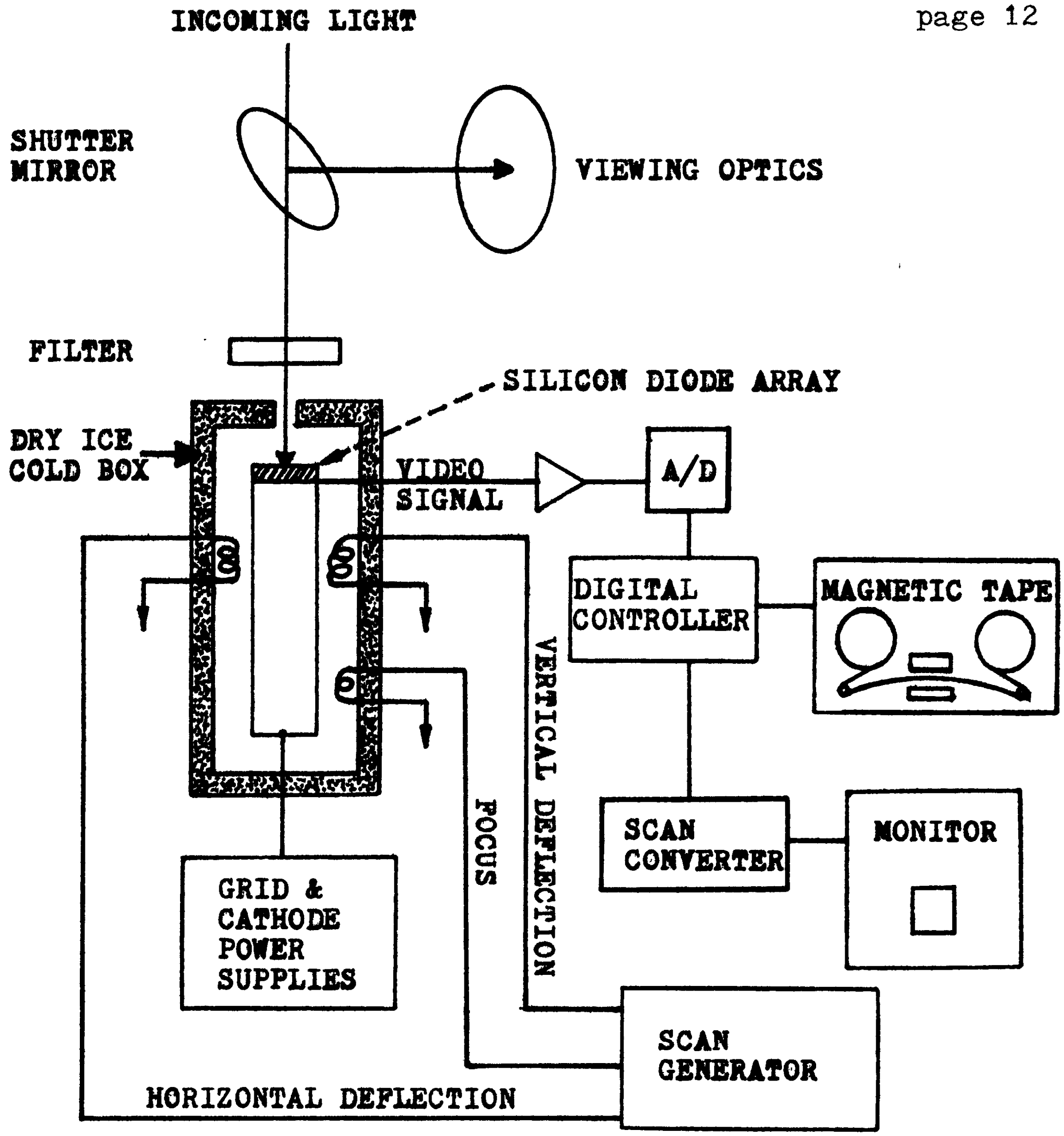

Figure 1. A schematic diagram of the Vidicon Imaging System.

amount of charge lost during exposure. Implicitly this current is a video signal. It is amplified, digitized and recorded on magnetic tape as a matrix of integer intensity values, 250 rows by 256 columns. A sample of a vidicon image of Mars is displayed in Figure 2. Half the planet in its digital format can be seen. Each number represents an intensity value derived from the video signal as the scanning electron beam recharged four diodes in the silicon diode array. Such images can be projected onto film for study and display. Furthermore, with corresponding darkfield and flatfield images, each planetary image can be processed to yield spectral reflectivity data.

MARS6136

	117	118	119	120	121	122	123	124	125	126	127	128	129	130	131	132	133	134	135	136	137	138	139	140	141
18-	263	261	258	252	254	261	255	251	255	258	265	259	254	255	255	259	251	246	255	263	255	254	255	263	265
19-	250	267	265	271	257	254	255	265	255	253	266	261	255	255	255	263	261	255	240	265	265	252	255	263	259
20-	266	266	261	263	255	268	269	259	263	258	263	260	265	262	263	266	258	259	259	268	257	265	255	267	261
21-	255	255	266	252	260	255	263	258	255	258	264	263	261	255	253	261	255	263	255	255	260	258	246	255	253
22-	271	287	281	272	265	261	274	258	264	263	262	263	257	257	255	267	268	251	266	264	258	260	252	255	261
23-	385	385	382	364	339	320	314	292	272	275	273	273	271	265	255	276	261	261	254	262	273	257	264	263	261
24-	685	703	688	655	606	547	499	451	406	342	305	283	269	257	249	258	264	260	255	261	263	255	258	257	258
25-	1004	1010	1010	1004	993	1005	1056	1082	1005	809	590	421	318	279	272	267	259	254	261	265	261	269	264	255	259
26-	1158	1170	1175	1183	1228	1397	1747	2087	2193	1912	1363	837	520	374	306	282	281	266	274	272	261	264	272	255	264
27-	1240	1257	1261	1279	1337	1517	1969	2561	2938	2734	2061	1362	863	560	396	307	287	275	265	282	273	259	263	263	260
28-	1255	1259	1276	1297	1338	1452	1645	1985	2266	2229	1912	1524	1139	811	566	399	305	288	277	265	264	257	271	261	269
29-	1242	1261	1279	1309	1340	1402	1457	1535	1615	1648	1617	1520	1350	1099	837	586	417	322	288	273	277	268	273	280	263
30-	1239	1265	1279	1324	1355	1384	1422	1466	1490	1512	1542	1546	1549	1432	1196	891	615	409	323	284	255	263	270	275	269
31-	1271	1286	1311	1337	1359	1388	1411	1424	1443	1482	1532	1629	1733	1718	1563	1265	906	600	410	325	286	276	260	263	258
32-	1287	1321	1351	1375	1398	1417	1432	1441	1450	1468	1539	1668	1816	1908	1869	1663	1301	921	608	408	312	280	274	269	271
33-	1320	1349	1366	1402	1416	1451	1451	1447	1445	1477	1535	1649	1858	2005	2082	2041	1782	1384	950	605	388	307	283	274	277
34-	1322	1352	1378	1394	1428	1455	1469	1461	1456	1466	1547	1664	1856	2051	2223	2332	2296	1991	1483	944	569	374	294	285	264
35-	1335	1365	1389	1406	1435	1464	1476	1494	1483	1492	1549	1644	1840	2048	2272	2480	2635	2548	2071	1406	832	483	341	295	288
36-	1341	1358	1381	1409	1460	1484	1498	1499	1502	1517	1548	1644	1808	2017	2259	2513	2760	2864	2544	1831	1094	617	389	308	279
37-	1316	1367	1398	1437	1472	1489	1524	1535	1522	1520	1560	1619	1775	1979	2232	2505	2784	2981	2808	2110	1294	730	442	331	284
38-	1385	1425	1468	1518	1547	1573	1587	1568	1559	1539	1565	1590	1692	1868	2118	2397	2693	2915	2816	2155	1388	815	493	349	289
39-	1416	1461	1518	1578	1635	1670	1664	1640	1609	1584	1577	1583	1662	1793	2032	2287	2540	2758	2654	2109	1404	840	505	357	305
40-	1419	1480	1539	1616	1668	1726	1742	1693	1638	1615	1610	1632	1687	1785	1974	2192	2430	2605	2512	2040	1399	861	521	362	294
41-	1452	1505	1573	1642	1712	1772	1795	1732	1654	1607	1605	1639	1712	1783	1902	2067	2248	2406	2373	1988	1405	681	544	367	314
42-	1462	1510	1565	1623	1707	1781	1804	1756	1670	1624	1622	1666	1751	1815	1904	2011	2137	2256	2252	1921	1371	877	547	380	310
43-	1463	1497	1539	1588	1663	1762	1788	1741	1655	1607	1632	1708	1780	1821	1867	1946	2061	2161	2115	1806	1311	850	535	368	309
44-	1465	1504	1539	1585	1659	1732	1777	1714	1650	1637	1683	1773	1860	1894	1918	1948	2005	2096	2058	1729	1240	808	522	368	300
45-	1495	1530	1541	1592	1653	1715	1731	1689	1632	1649	1746	1835	1921	1959	1980	1958	1990	2055	1990	1654	1175	771	503	364	306
46-	1480	1503	1535	1587	1638	1701	1724	1673	1624	1657	1758	1854	1946	1961	1949	1924	1935	1994	1912	1541	1079	702	457	343	290
47-	1480	1502	1511	1549	1614	1696	1737	1697	1662	1693	1776	1856	1936	1917	1859	1815	1838	1921	1775	1372	948	625	429	336	296
48-	1462	1479	1516	1543	1601	1689	1745	1715	1678	1695	1751	1813	1893	1847	1754	1714	1777	1833	1616	1201	826	554	400	316	290
49-	1429	1455	1482	1519	1568	1654	1735	1744	1705	1697	1713	1764	1799	1744	1651	1626	1724	1708	1416	1022	700	483	356	296	278
50-	1417	1421	1453	1483	1559	1668	1763	1801	1793	1772	1776	1793	1791	1697	1642	1656	1691	1532	1181	844	584	421	337	292	270
51-	1396	1411	1456	1511	1597	1681	1780	1841	1834	1828	1831	1831	1779	1693	1663	1701	1640	1331	976	695	485	374	319	282	275
52-	1428	1463	1520	1580	1656	1746	1840	1906	1929	1941	1916	1884	1842	1813	1863	1828	1552	1149	803	563	410	330	288	279	274
53-	1421	1442	1517	1602	1708	1791	1881	1943	1965	1967	1952	1936	1953	2012	2047	1815	1356	944	646	463	359	313	280	272	272
54-	1400	1433	1502	1594	1697	1809	1871	1915	1953	1983	2007	2030	2098	2097	1931	1489	1043	729	521	403	334	305	288	277	275
55-	1389	1436	1498	1585	1680	1767	1837	1878	1914	1964	2020	2084	2124	1902	1501	1089	777	565	428	333	293	281	272	265	267
56-	1347	1397	1467	1535	1621	1681	1724	1760	1823	1893	1959	1933	1708	1336	1014	762	567	435	347	304	281	271	271	269	273
57-	1367	1399	1444	1492	1552	1583	1613	1645	1697	1709	1632	1400	1133	893	705	543	433	353	307	297	278	276	278	271	270
58-	1445	1432	1444	1455	1464	1453	1466	1444	1377	1264	1091	903	745	613	497	416	357	314	287	287	280	271	274	273	273
59-	1555	1501	1457	1392	1341	1272	1171	1071	954	843	725	621	530	449	381	337	302	283	267	276	261	274	270	270	269
60-	1552	1417	1292	1140	1037	925	831	740	654	580	517	454	392	340	325	293	282	283	275	271	272	267	268	265	265
61-	1023	939	846	761	697	632	580	519	469	423	384	347	323	298	281	276	276	275	279	274	278	264	260	267	260
62-	634	603	551	519	473	449	419	370	349	326	310	294	272	269	266	275	258	251	259	259	259	259	260	255	263
63-	435	413	403	376	357	350	331	305	297	297	284	277	260	264	263	269	265	264	265	265	262	266	264	270	262
64-	340	322	313	295	292	301	296	278	259	266	276	277	269	267	259	267	267	265	268	263	261	263	269	276	265
65-	278	281	270	278	273	272	263	271	269	279	263	267	254	262	268	262	265	255	267	255	262	263	255	255	255
66-	268	269	268	264	263	266	268	255	258	263	270	273	264	261	275	271	255	255	266	255	263	259	272	268	266
67-	254	265	269	262	265	269	264	271	265	263	276	271	262	255	255	265	266	266	273	277	263	267	259	263	270

Figure 2. Part of a vidicon image of Mars.

III. Images of the 1973 Mars Dust Storm

The major Martian dust storm of 1973 made its appearance on October 13 over the usually dark area, Solis Lacus (Capen, 1973). An analysis of International Planetary Patrol photographs (Martin, 1974) captures the dramatic history of this planet-wide disturbance. For several days following its inception, the storm expanded rapidly, ultimately obscuring the entire Martian surface. This obscuration diminished over a period of weeks. The images presented here refer specifically to a four hour segment of Day 2 of the dust storm, October 14, 1973. A map of the storm as it appeared on Day 2 can be seen in Figure 3.

The first images of the storm were taken at around 9:00 Universal Time, a few hours after Solis Lacus passed through the dawn terminator. Successive images followed the progress of the storm during the ensuing 4 hours. Samples from amoung the 100 vidicon images taken comprise the photographs exhibited in Figures 4 and 6.

Figure 4 is a display of images observed through a blue filter (0.40 microns). The contrast in the images has been varied to enhance the features. The north polar hood crowns the top of the planet and the smaller south polar cap appears

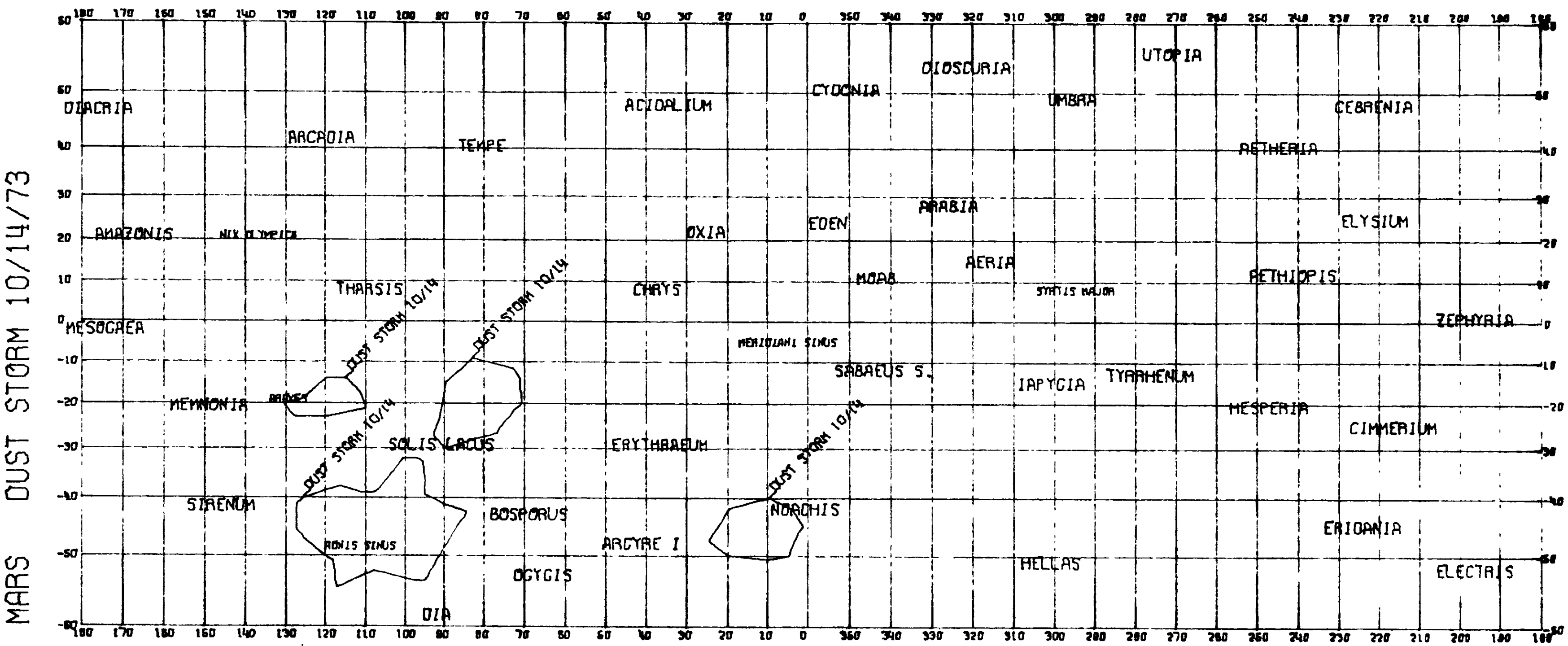

Figure 3. Mercator projection of Mars with boundaries of the dust storm on October 14, 1973, from Martin (1974).

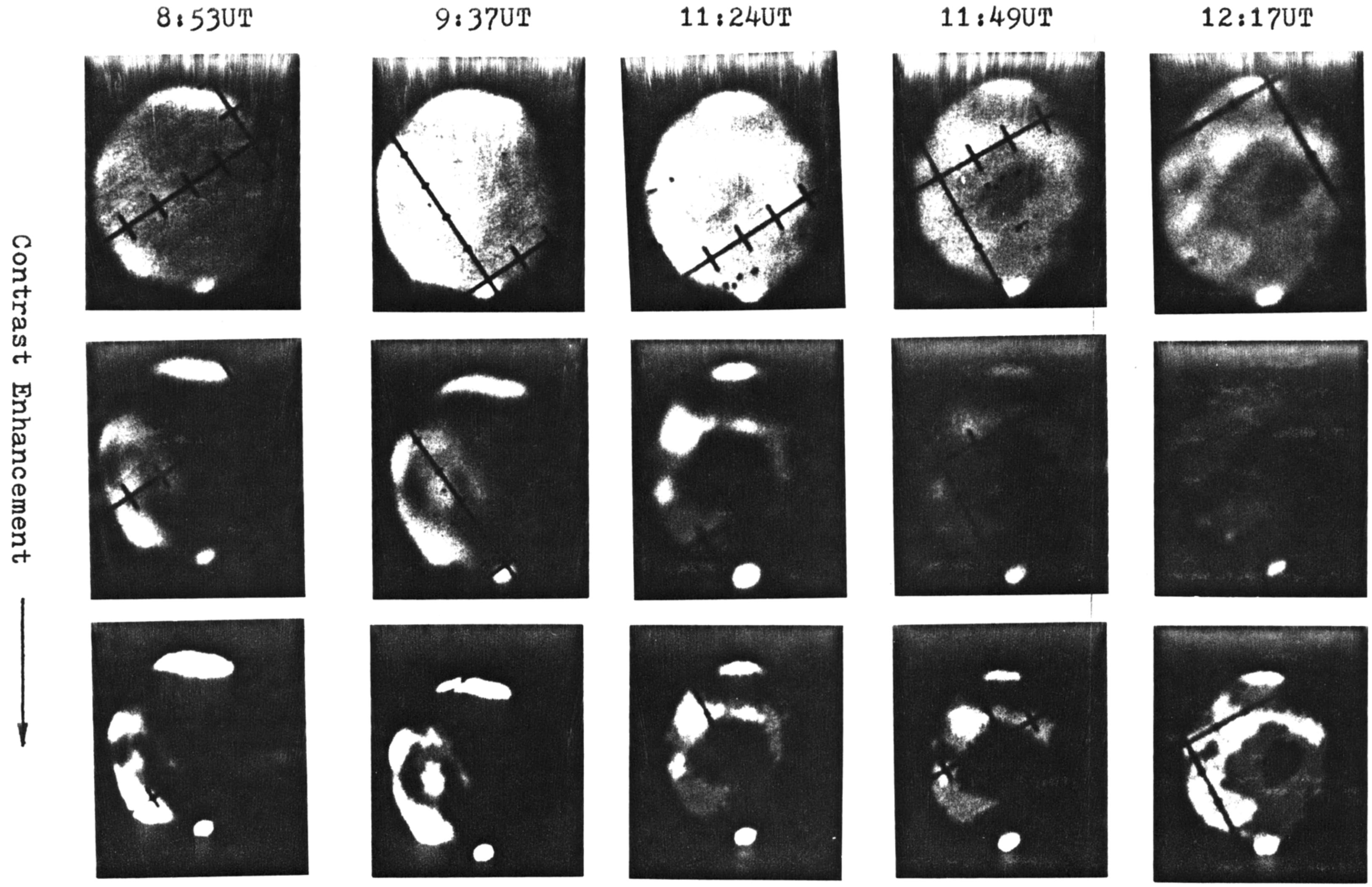

Figure 4. Photographs of vidicon images of Mars taken through a 0.40 micron filter. Time is Universal Time, Oct. 14, 1973 - Day 2 of the storm.

at the bottom of each image. The remaining visible features in these blue images reveal the sprawling expanse of the storm system orly a day after it was first noted. A chronicle of short term phenomena is clearly present. To assist in associating elements of the dust storm with place names on Mars, disk maps of the planet are presented in Figure 5 to show the visible face of Mars as it appeared for the first and last images in Figure 4.

Solis Lacus (25°S, 80°W) is at the bull's eye formed by the ring of clouds. Its bright appearnace vanishes completely in the blue as the dust storm progresses toward the sub-solar meridian. Even more spectacular is the brilliant cloud over the Aonis Sinus region (47°S, 107°W) southwest of Solis Lacus. This cloud fades significantly between 9:37UT and 11:24UT along with the Solis Lacus cloud. The sudden regression from brilliance in the blue in both of these clouds is thought to be evidence of volatiles (*) which, having condensed onto suspended dust particles during the Martian night, appear bright in the morning light and then fade away as exposure to solar radiation causes sublimation. Furthermore, dehydroxylated goethite has been proposed as a constituent of the Martian

(*) Huguenin (1975)
Abramenko and Prokof'eva (1975)
Leovy et al (1972)
Smith and Smith (1972)
Baum (1974)

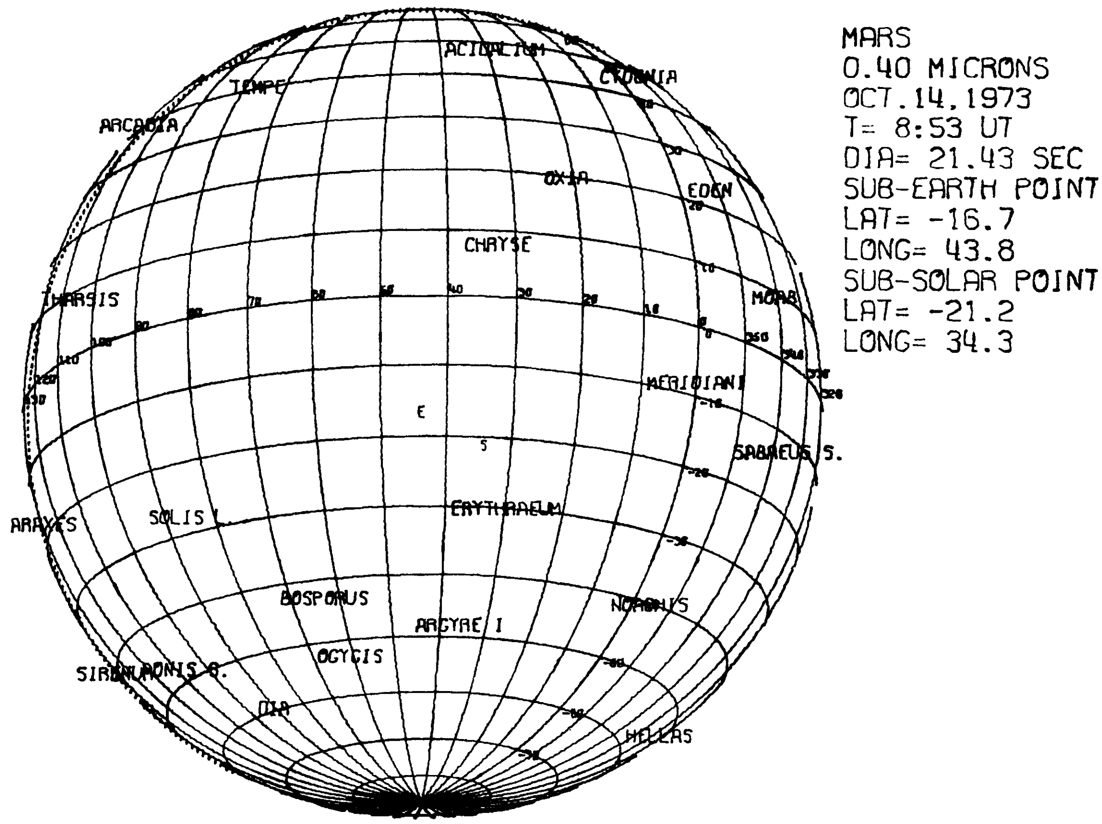

Figure 5. Above is first, below is last of 0.40 micron images.

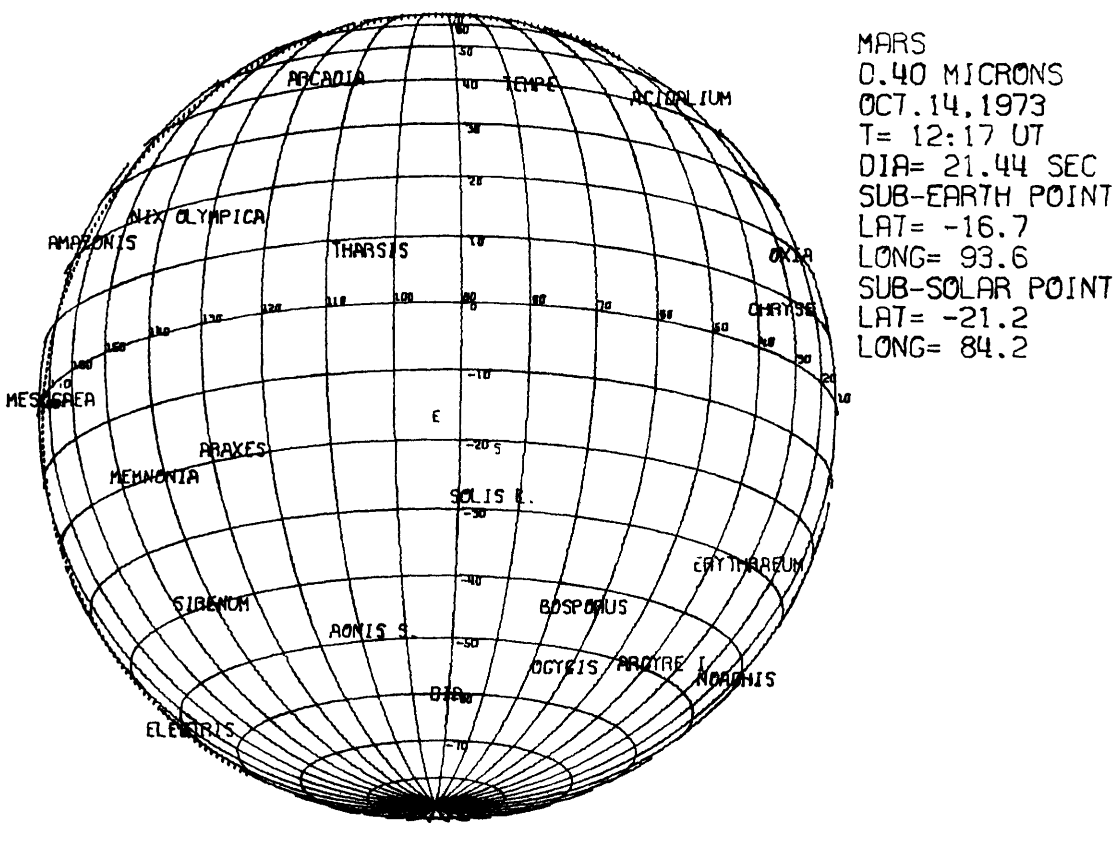

soil (Huguenin, 1974). This mineral, according to Huguenin (1975), in a dust grain can adsorb water, increasing the specific surface of the grain and thereby raising the reflectivity of the grain. Exposure to sunlight is sufficient to knock off the attached water molecules.

The third large cloud visible in the blue images lies over western Tharsis (10°N, 120°W). Unlike the clouds over Solis Lacus and Aonis Sinus, the Tharsis cloud remains bright in the blue throughout the observation period, although it appears to fade somewhat. Brightenings over this area of Mars have been, as a result of observations by Mariner 9 (Leovy et al, 1972), associated with clouds forming on the leeward side of the four large Tharsis volcanos. The dust storm map in Figure 3 indicates that this large, bright cloud is unconnected with the dust storm further south. The boundaries, however, of the storm in Figure 3 were determined primarily using photographs of Mars taken through a red filter. As will be seen shortly (Figure 6), this technique reveals the centers of dust concentrations. Images taken through a blue filter apparently show the more tenuous reaches of the storm due to condensed and adsorbed volatile brightening. The general dustiness of the Martian atmosphere expected during dust storm conditions, combined with reflective volatiles coating the particles, may be enlarging and/or highlighting what might normally be a few small clouds around the volcanos. The fact that this large and bright cloud remains bright during the full extent of the observation period, whereas the Solis Lacus and Aonis Sinus clouds vanish, may be (1) an indication that it is a different kind of cloud (i.e. a leeward wave cloud system - see Leovy et al, 1972, and Smith and Smith, 1972), or (2) it has not yet been exposed to enough solar radiation to volatilize all the condensates. This second possibility will be discussed in more detail in the following analysis of the small Araxes cloud.

The map in Figure 3 indicates that westward of Solis Lacus there is a dust cloud over the Araxes region (20°S, 120°W). It appears very clearly as a bright patch beneath the Tharsis cloud in Figure 4 from 11:24UT onward. The Araxes dust cloud is further west than both the Aonis Sinus and Solis Lacus clouds. It therefore received during the imaging period less solar radiation than the other two dust clouds. If volatiles are indeed causing its luminescence, it is not surprising that the Araxes cloud remains bright as its two eastward companions vanish. The Araxes cloud can be expected to stay bright until it has absorbed sufficient sunlight to sublimate its condensed volatiles.

A fourth large dust cloud noted by Martin (1974) on Day 2 of the storm lies over Noachis (45°S, 15°W). As the maps in

Figures 3 and 5 indicate, the Noachis cloud, were it visible, would be seen near and on the east limb in all the images. But since no condensed or adsorbed volatiles can be expected to remain late into the Martian afternoon, this clouds' invisibility in the blue can be accounted for.

Finally, there are tenuous clouds directly north of Solis Lacus which remain bright long after the Solis Lacus cloud has been extinguished. This length of clouds is in the region of the Coprates Canyon. The topography in this system of canyons may be aiding the survival of adsorbed and condensed volatiles adhering to the dust particles.

In contrast to the images exposed through the 0.40 micron filter, images taken through a red filter tell a different story. A 0.73 micron filter was used for the images displayed in Figure 6. Each of these was exposed a few minutes after the corresponding blue images in Figure 4. Contrast enhancement has again been applied to bring out the significant features of the dust storm at this red wavelength. Northwest of Solis Lacus can be seen the bright Tharsis region. The rectangular Mare Erythraeum as well as (in the later images) the protruding finger of Mare Sirenum are the dark regions to either side of the storm. The bright knot of the main dust cloud masks Solis Lacus. It appears in the highly contrasted images as an

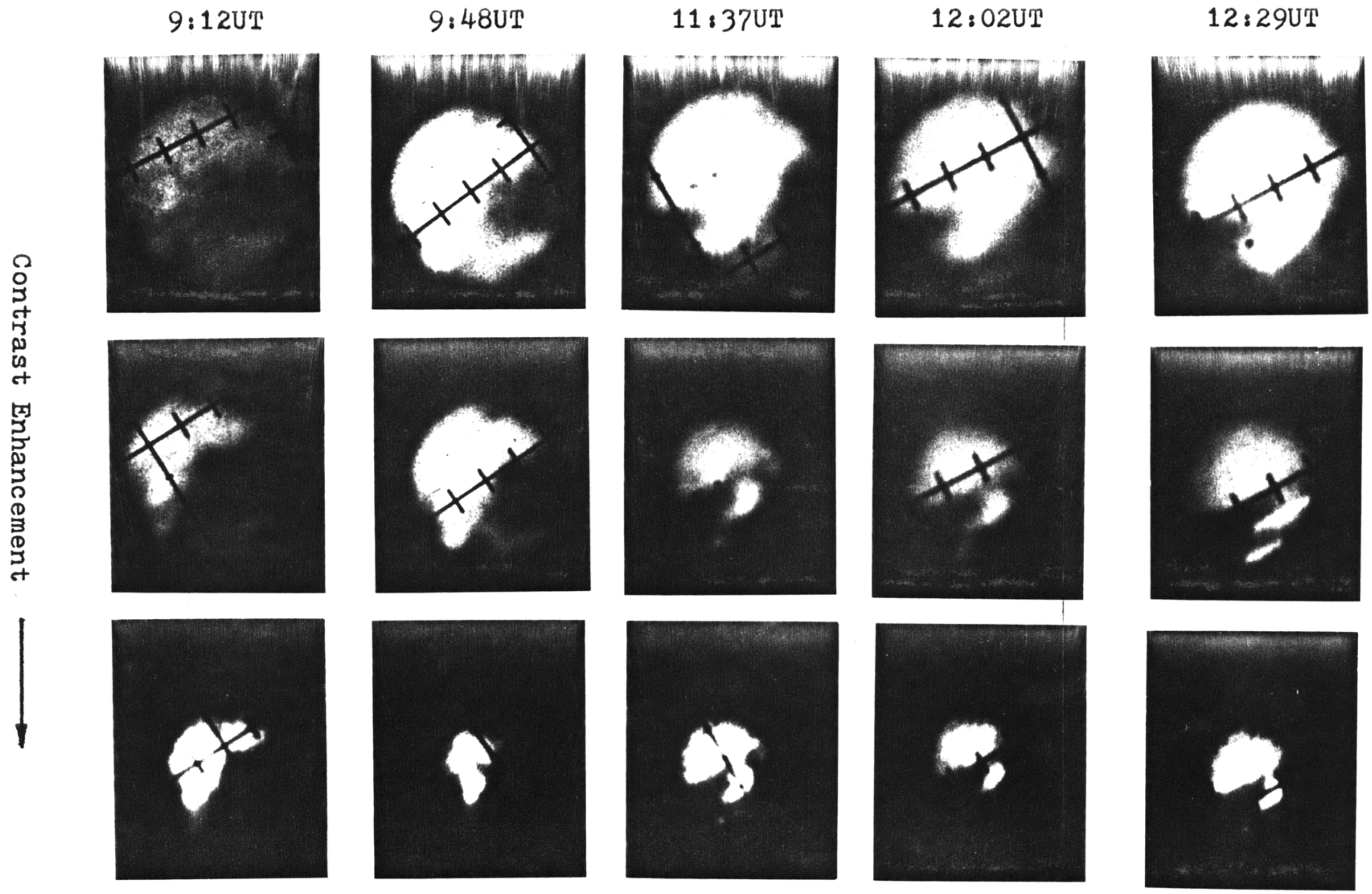

Figure 6. Photographs of vidicon images of Mars taken through a 0.73 micron filter. Time is Universal Time, Oct. 14, 1973 - Day 2 of the storm.

appendage at the bottom of the dome-shaped bright region to the northwest of Solis Lacus. The disk maps in Figure 7 show the planet as it appeared for the first and last images in Figure 6.

The dust cloud over Solis Lacus appears bright throughout the 4 hour observation period whereas in the blue images the storm fades as the Martian day proceeds. The transient brightenings in the blue have been attributed to condensed and adsorbed volatiles. The constant brightness of the storm in the red indicates that the red dust particles themselves have been imaged. They are bright area material that has been swept up by the local winds. No 'dark' dust storms - composed of dark area material - have ever been observed on Mars. Apparently the bright area material is much more fine-grained than dark area material and hence more easily windborn (see Hugeunin (1974) for a discussion of particle size origins and further references).

The dust cloud over Aonis Sinus to the southwest of Solis Lacus and the dust cloud over Araxes to the west are both much weaker at 0.73 microns than the Solis Lacus cloud. The Araxes cloud cannot be distinguished in the photographs in Figure 6 although it is barely perceptible in the original vidicon images when displayed on a viewing screen. The Aonis Sinus cloud is faintly apparent in Figure 6 and weakens as the

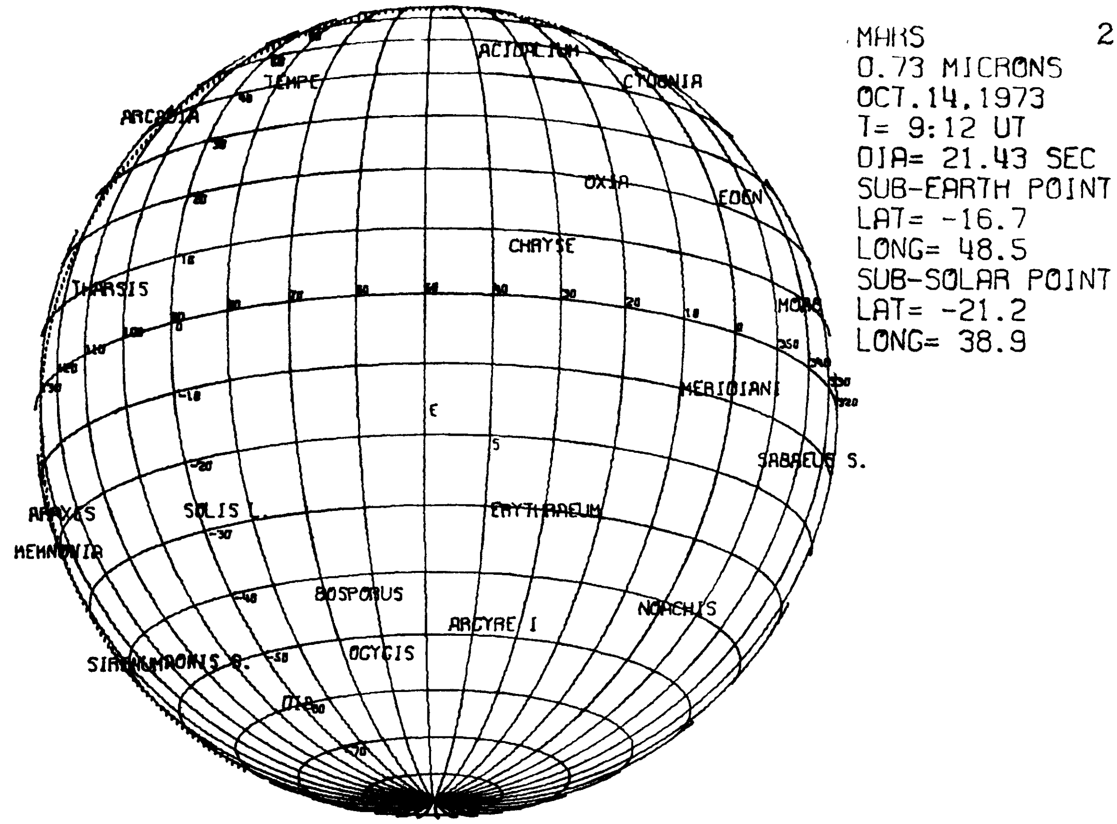

Figure 7. Above is first, below is last of 0.73 micron images.

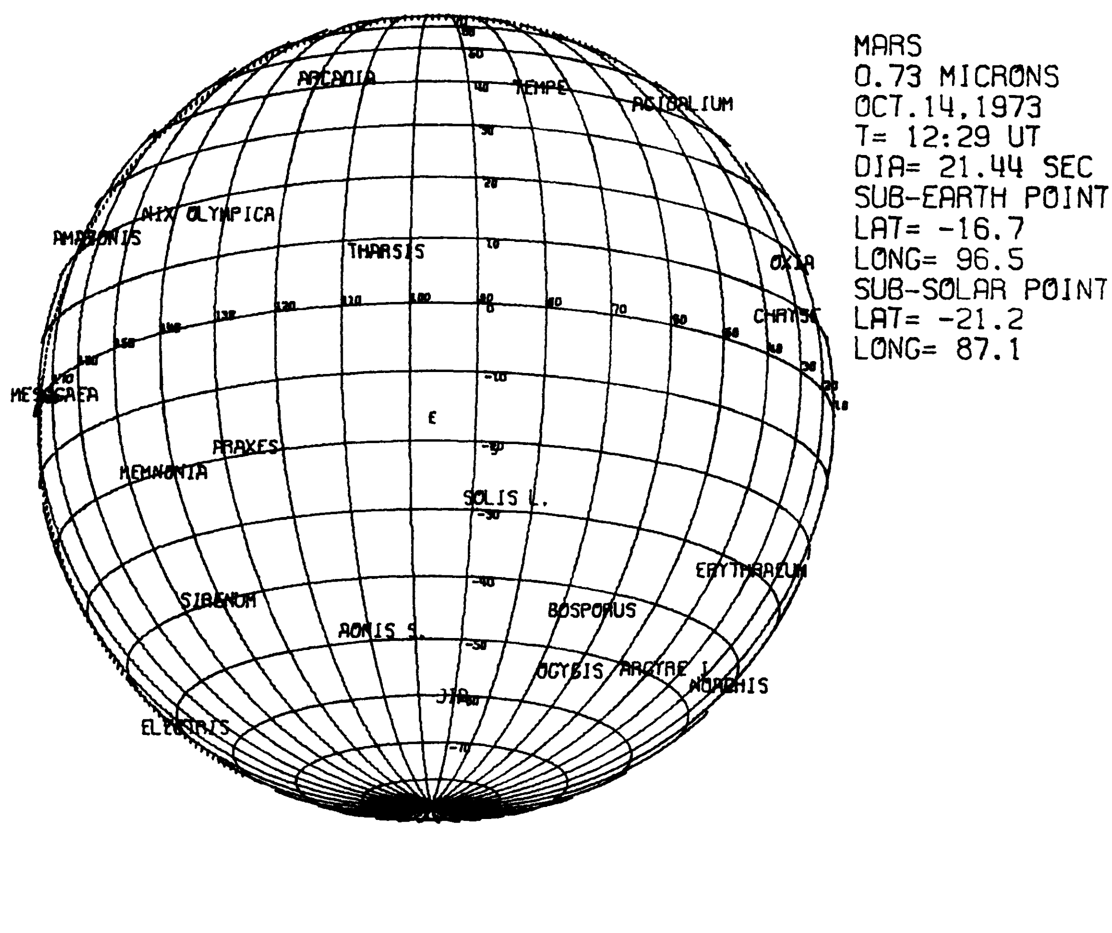

contrast is increased. Presumably the concentration of dust in the disturbance over Solis Lacus was, on Day 2 of the storm, greater than the concentration of dust particles in the other two westward storm clouds.

In the highest contrasted images at 0.73 microns the Aonis Sinus cloud reveals an interesting feature. A small spot appears beneath the tail of the comma-shaped Solis Lacus cloud. This feature is evident at 11:37UT and later but not earlier at 9:48UT or 9:12UT. The apparent brightening of this cloud at 11:37UT may be an artifact caused by the contrast enhancement process, or it might be a real event caused by a rapid increase in the local concentration of dust. The area of the bright spot is about 60,000 square kilometers.

The cloud over western Tharsis, which appeared so large and bright in the blue, is not distinguishable in the red. This supports the contention, already put forward, that the Tharsis cloud is not composed primarily of dust.

The cloud over Noachis, which was not seen in the blue, does not appear in the red either. This cloud was not evident to Martin (1974) the next day, October 15 (see Figure 15 for a map of the dust storm as it appeared on October 15). That the Noachis cloud is not seen here in the red and that it vanished altogether by the next day are indicative of its tenuous nature. The concentration of dust over Noachis was probably small and diminishing.

Since the bright knot of dust over Solis Lacus is both confined and pronounced in the highly contrasted images in Figure 6, an attempt was made to measure any change in the area covered by this specific cloud. By calculating the projected surface area associated with each picture element (pixel) that could be assigned to the Solis Lacus cloud, the total area of this storm cloud can be determined for any specified image. During the short imaging period (4 hours) no detectable changes in the area of the Solis Lacus cloud were discovered. This is not an unexpected result. Gierasch and Goody (1973) and Leovy, Zurek and Pollack (1973) have described opposing mechanisms for Martian dust storm formation. Both, however, estimate that a wind speed of 30 m/sec. is not unreasonable during the growth of such a storm. Over a four hour period this wind speed could move dust slightly more than 400 kilometers. Each pixel near the center of a vidicon image of Mars represents an area about 200 km. across. Therefore, over the 4 hour imaging period a cloud of dust expanding at 30 m/sec. would not necessarily be detected. The resolution of the images simply is not fine enough to determine wind speeds even in the extreme conditions a Martian dust storm imposes.

A general expansion of the total storm system as the clouds rotate eastward is suggested by the images in Figure 4. This apparent expansion may be accounted for by the distortion caused by projecting the spherical planet onto the image plane. A feature near the limb of the planet will grow in apparent size as it is rotated toward the sub-earth point. To equalise this distortion and search for any changes in the gross morphology of the entire storm system, and to uncover possible changes in cloud structure that may not effect the integrated area of any particular cloud, the digital vidicon images in Figures 4 and 6 were artificially rotated to place Solis Lacus at the center in each rotated image. A flowchart of the Rotation program is in Figure 8. The rotated images are shown in Figure 9 (blue images) and Figure 10 (red images).

The general expansion of the total storm that appeared in the original images at 0.40 microns (Figure 4) is no longer evident in the corresponding rotated images (Figure 9). In particular, the cloud over Solis Lacus, which seems to grow in size from 8:53UT to 9:37UT in Figure 4, remains constant in size in the distortion equalized images at 8:53UT and 9:37UT in Figure 9. The overall morphology of the dust storm remains uniform while the rapid changes in brightness occure.

However, possible changes in cloud structure appear in Figure 10. In the highly contrasted versions of the rotated images the dust cloud over Solis Lacus appears at 11:37UT,

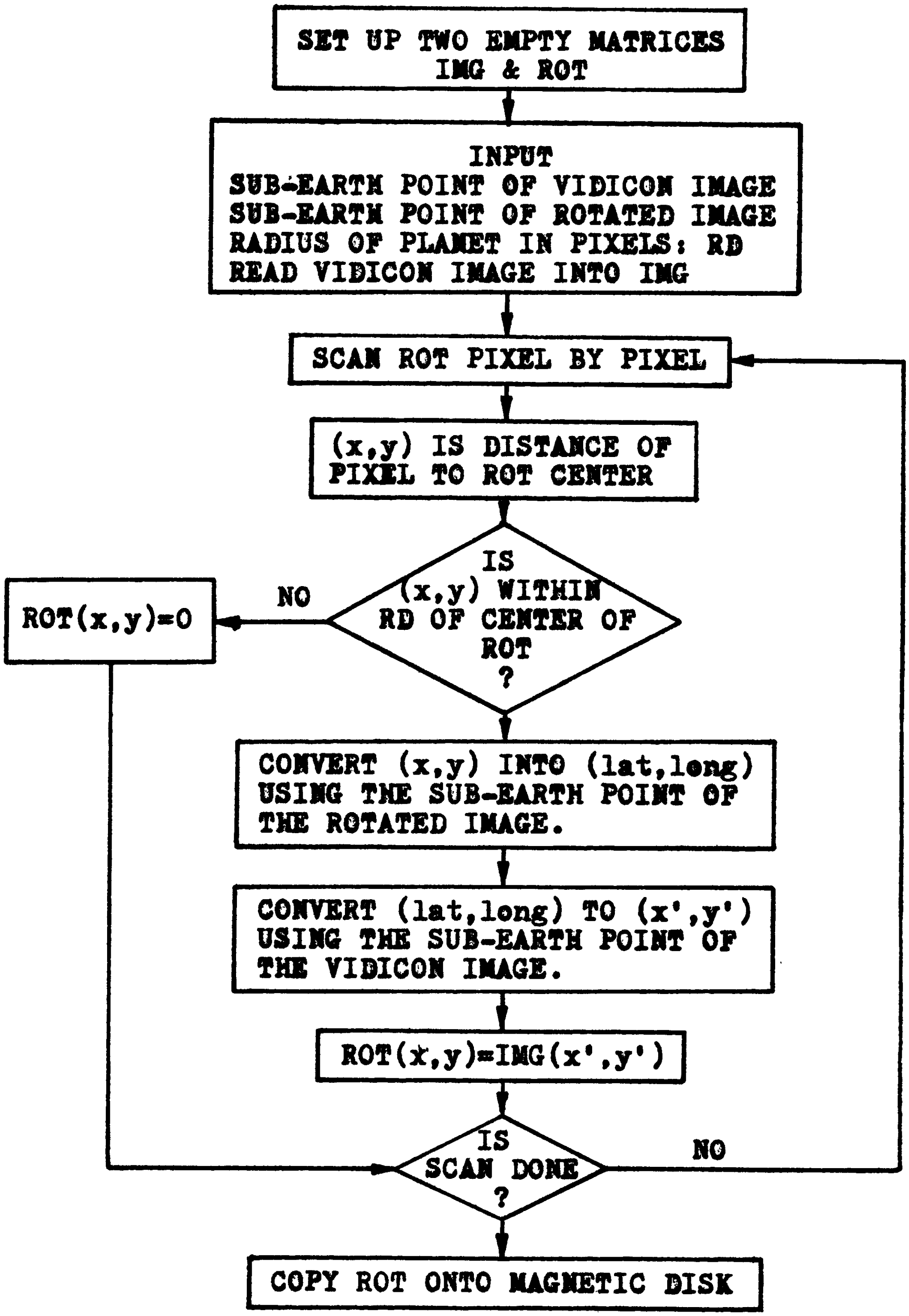

Figure 8. Flowchart of Rotation program.

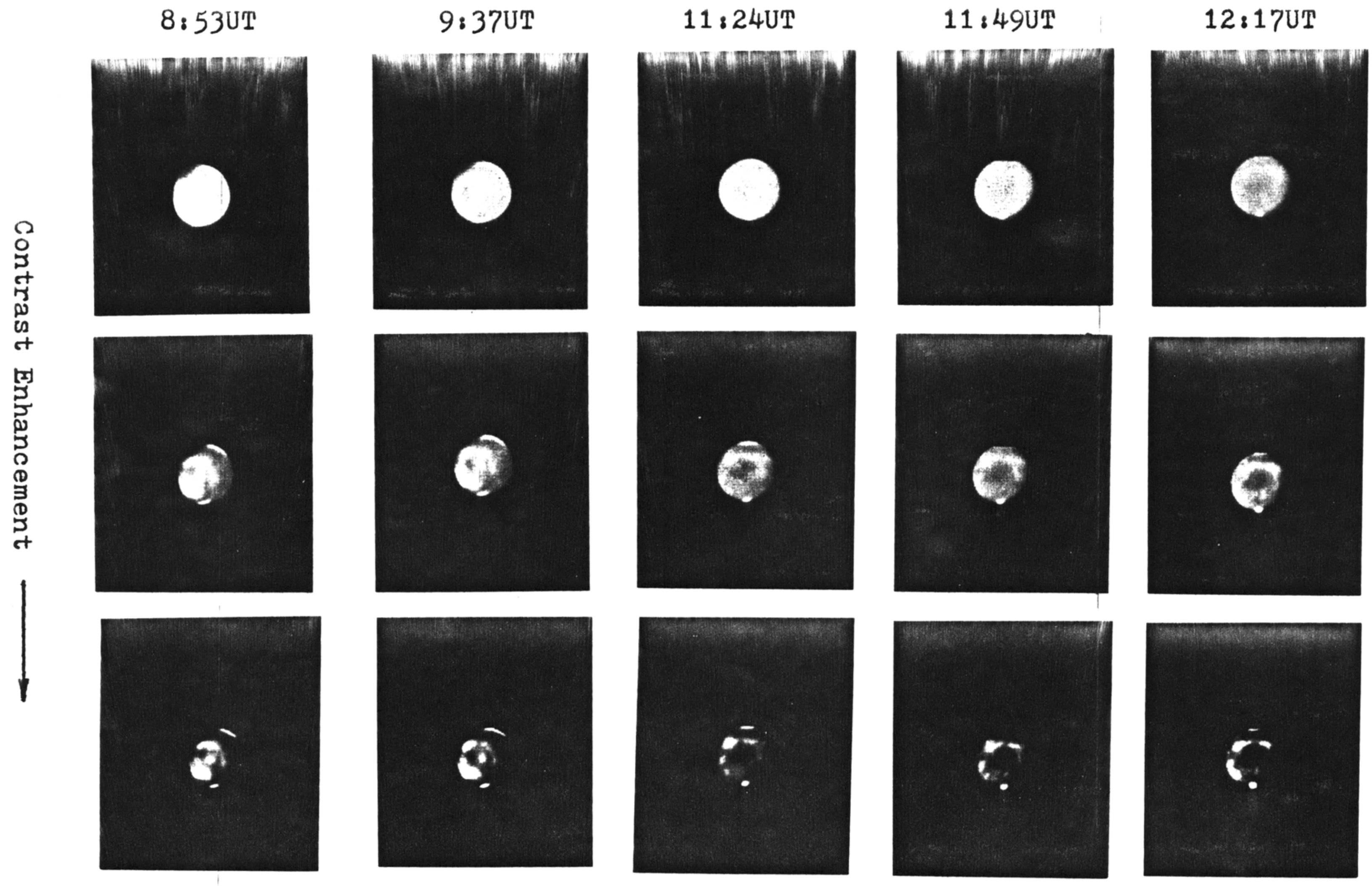

Figure 9. Photographs of rotated vidicon images of Mars taken through a 0.40 micron filter. The center of the planet for every picture is Solis Lacus (20°S, 80°W).

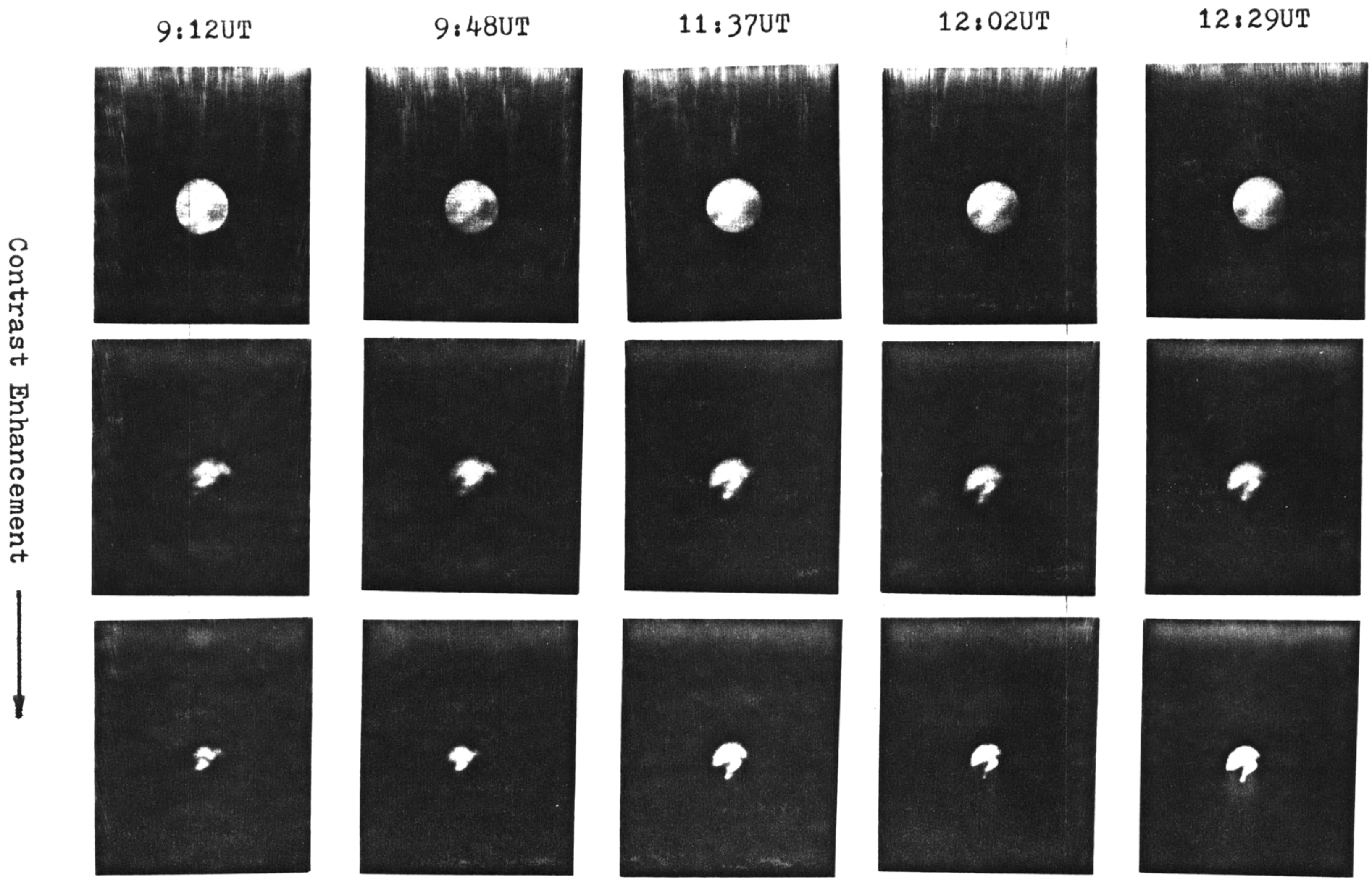

Figure 10. Photographs of rotated vidicon images of Mars taken through a 0.73 micron filter. The center of the planet for every picture is Solis Lacus (20°S, 80°W).

12:02UT and 12:29UT as a comma-shaped appendage beneath the dome-shaped Tharsis region to the north. The shape of this dust cloud appears slightly different at the two earlier times, 9:12UT and 9:48UT (see also the original images in Figure 6). If this apparent structural change is real, it may be associated with the appearance of the bright spot of dust over Aonis Sinus (discussed earlier). The Aonis Sinus spot appears as a 'period' below the 'comma' at 11:37UT and later (Figures 6 and 10).

The vidicon images of Mars, which by luck captured the Great Dust Storm of October, 1973, have revealed an abundance of information about the structure and diurnal development of the various clouds during the second day of the storm. The broad spectral coverage of the Vidicon Imaging System and the digital format of the images themselves aid in the analysis of rapibly changing features of both large and small scale. Much more information remains a part of these images and the following sections discuss the reduction and significance of this data.

IV. Image Processing

Since the analysis of the Mars vidicon images has, up to now, concerned only albedo features it has not been necessary to do any image processing (except for artificially rotating some of the images). Intrinsically, however, these images contain valuable photometric data from which spectral reflectivity curves can be constructed. Unlike a photographic plate, each diode in the silicon vidicon diode array responds (ideally) like a tiny photometer. Each picture element, i.e. each individual intensity value (as in Figure 2), can be thought of as a photometer data point for that particular area of the planet it covers and for that particular wavelength at which the image was exposed. To realize this data requires (1) the calibration of each image and (2) the derivation for each image of an accurate coordinate grid (in latitude and longitude, for instance) for the planetary disk. Mapping this grid onto the image associates picture elements with regions and features on the planet.

The calibration of the vidicon images is a two step process utilizing the existing batch image processing system (DIPSYS) developed at the M.I.T. Remote Sensing Laboratory. First, the images contain background noise caused by the dc bias in the video circuit and the backlighting from the electron beam filament. To eliminate this background a dark-field image is taken which is an image exposed like all other images except that the shutter remains closed. Subtracting the darkfield removes the background noise. Secondly, there are irregularities in the response of the diodes and in the filter transmissions across the face of the silicon diode array. Removal of these irregularities requires a flatfield, which is an image of uniform illumination (using, for instance, a de-focused Moon). After the darkfields have been subtracted from the data image and flatfield image, the data image is divided by the flatfield resulting in a calibrated image. Both of these two fundamental steps must be performed on each image. Figure 11 is a diagram of this calibration process.

Once the 100 data images from the October 14, 1973 Mars observations had been calibrated and saved on magnetic tape, a means had to be devised of producing a reflectance spectra for any desired location on the imaged face of the planet. Two subroutines for the DIPSYS image processing system were formulated to accomplish this goal.

Taking the original, uncalibrated images as a data base, a Center-Seeking program was written to find the unique row and column location of the center of each image and the mean radius of the planet in picture elements. In Figure 2, for example, the center is at ROW=43.72 COLUMN=118.56 and the

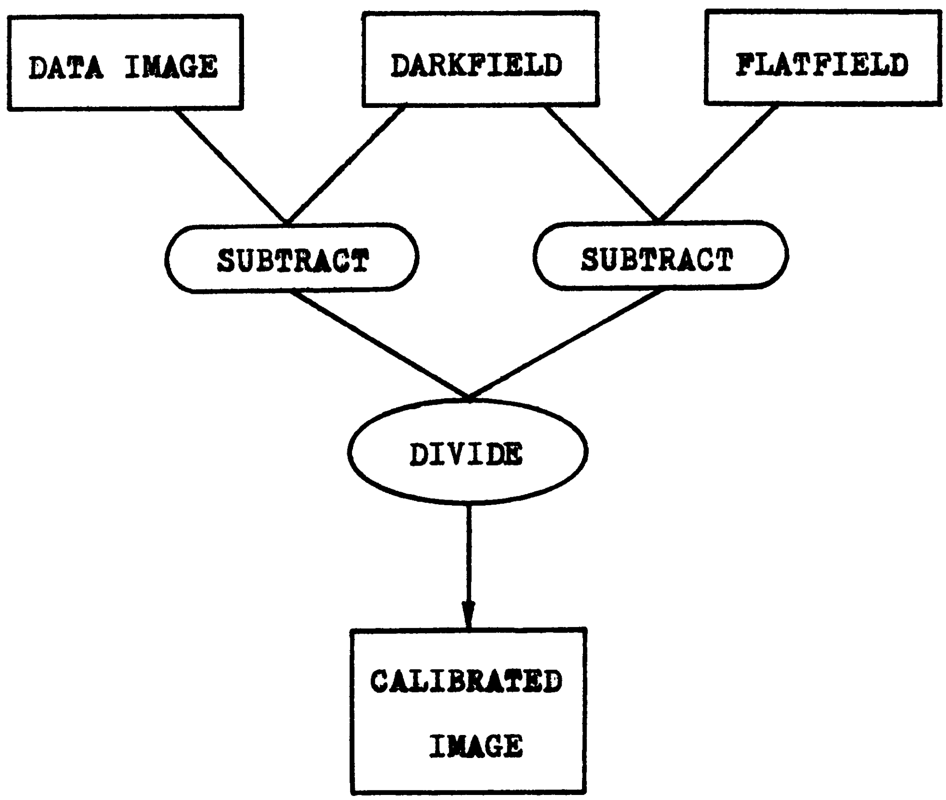

Figure 11. Calibration sequence for the vidicon images.

mean radius is 18.14 pixels. A flowchart of the Center-Seeking program is in Figure 12. Next a disk mapping program, already written by Doug Mink, provided the corresponding latitude and longitude location of the center of each image (see Figures 5 and 7 for examples). Using these two results as a data base, a Spot-Mapping program (Figure 13) was written to lift off of a vidicon image the average intensity value of all picture elements falling within a specified ellipse projected onto the image. Figure 18, for instance, shows disk maps of Mars with such ellipses thrown around areas under investigation. The Spot-Mapping program averages the intensity values within each ellipse.

Intensity values returned by the Spot-Mapping program can be treated exactly like photometer data. During an actual observation run with a photometer, the instrument returns data from some spot on Mars, and due to guiding problems, that spot drifts around within some elliptical boundary. By mapping that boundary onto calibrated vidicon images, the Spot-Mapping program simulates the return of photometer data.

The intensity values thus derived are plotted as a function of wavelength to produce reflectance spectra. These spectra are generally normalized to 1.0 at 0.56 microns. Furthermore, to reduce the adverse effects of seeing conditions and changing airmass during the observation period,

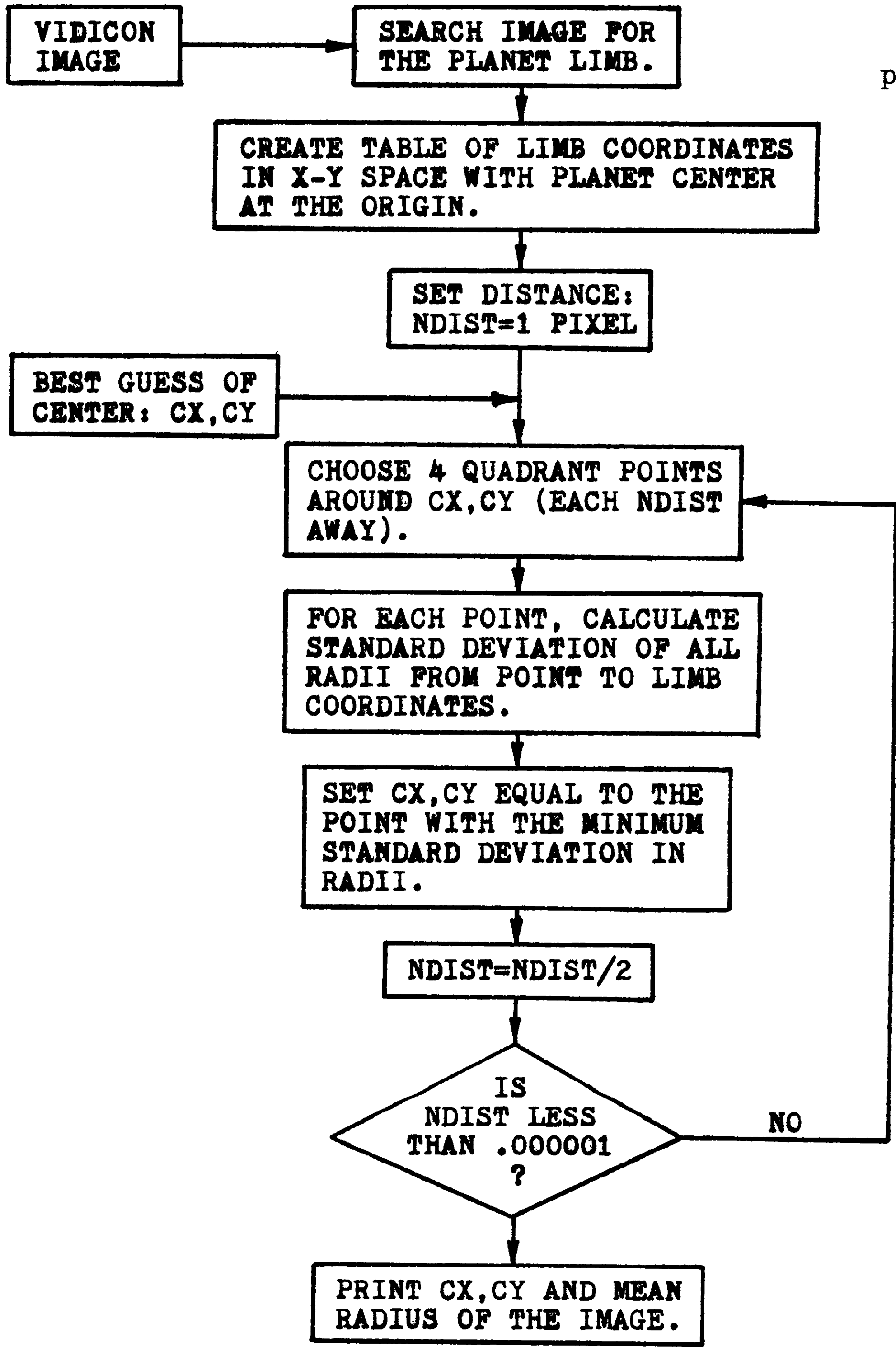

Figure 12. Flowchart of Center-Seeking program.

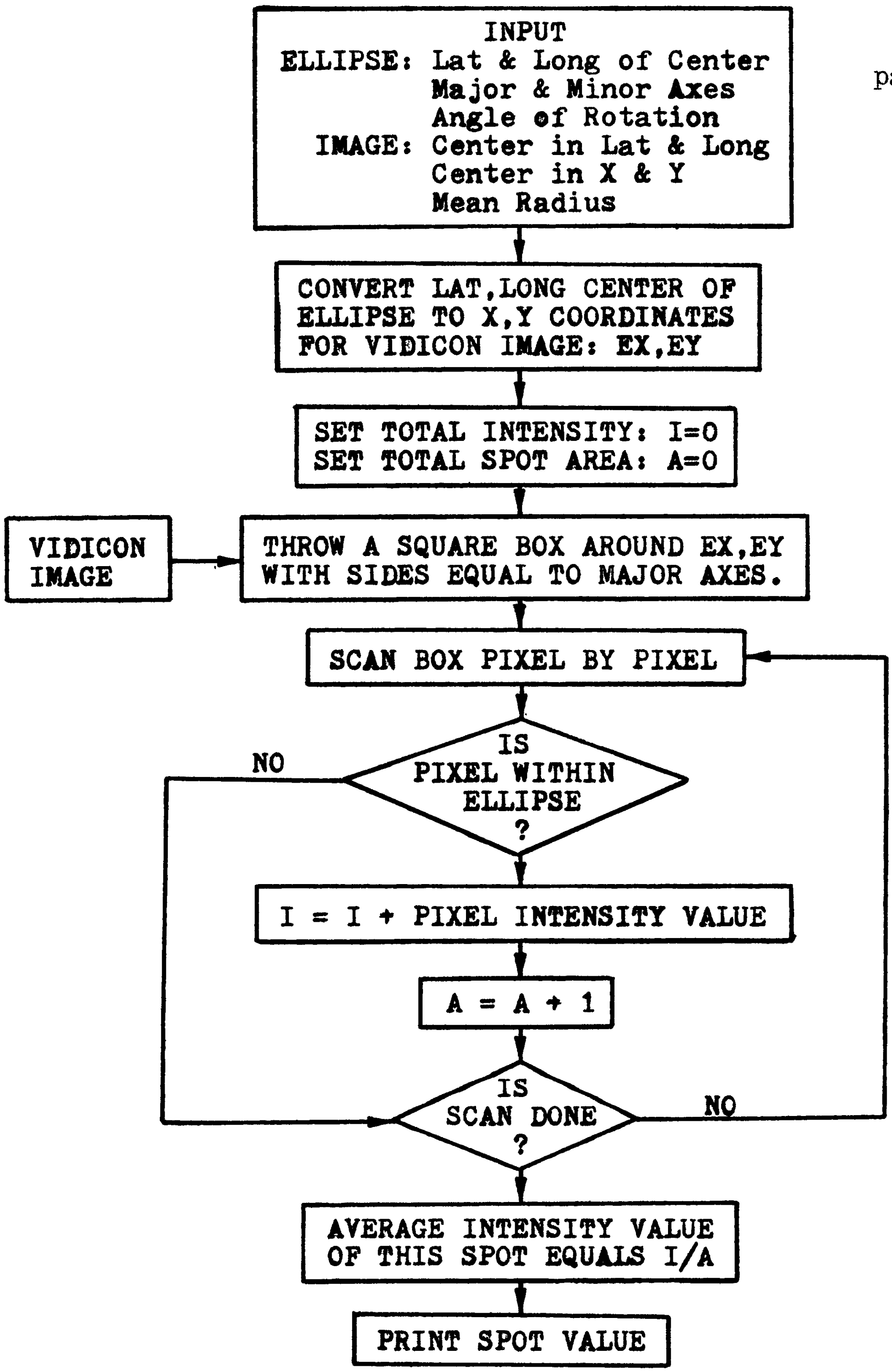

Figure 13. Flowchart of Spot-Mapping program.

relative reflectance spectra are obtained by dividing the normalized reflectance spectra for one area of the planet by the normalized reflectance spectra of another area on the planet. Following these reductions a comparison can be made between actual photometer data and the vidicon image data. Such a comparison would verify both the accuracy of the image processing system, particularly the Spot-Mapping program, and the photometric quality of the vidicon images.

V. Comparison of Relative Spectral Reflectivity Data

During the night of October 14, 1973 vidicon images of Mars were taken using twenty narrow-band filters ($\Delta\lambda$=250 Å). The spectral region from 0.35 microns to 1.03 microns was covered. Associated darkfields and flatfields were also imaged. On October 15, 16, and 19 a photometer system was used to probe numerous areas on the surface of Mars. Twenty six filters were used spanning the spectrum from 0.30 microns to 1.10 microns. About twenty five different areas on Mars (refered to as 'spots') were measured by the photometer during its three nights of observations. Figure 14 is a map of Mars showing the extent of the dust storm on October 14, the night the vidicon images were exposed. The ellipses define the twelve photometer spots that will be discussed. Figures 15, 16 and 17 are maps of Mars with the extent of the dust storm shown for October 15, 16 and 19 respectively. The ellipses are the boundaries within which (with 90% confidence) the photometer apeture was guided. Spot 4 and Spot 6 were taken on October 15 (Figure 15). Spots 7A through 15 were observed on October 16 (Figure 16). Spot 17 and Spot 20 were measured on October 19 (Figure 17). Also, Figure 18 shows disk maps of Mars which display the twelve photometer spots as viewed on the first and last of the vidicon images taken on

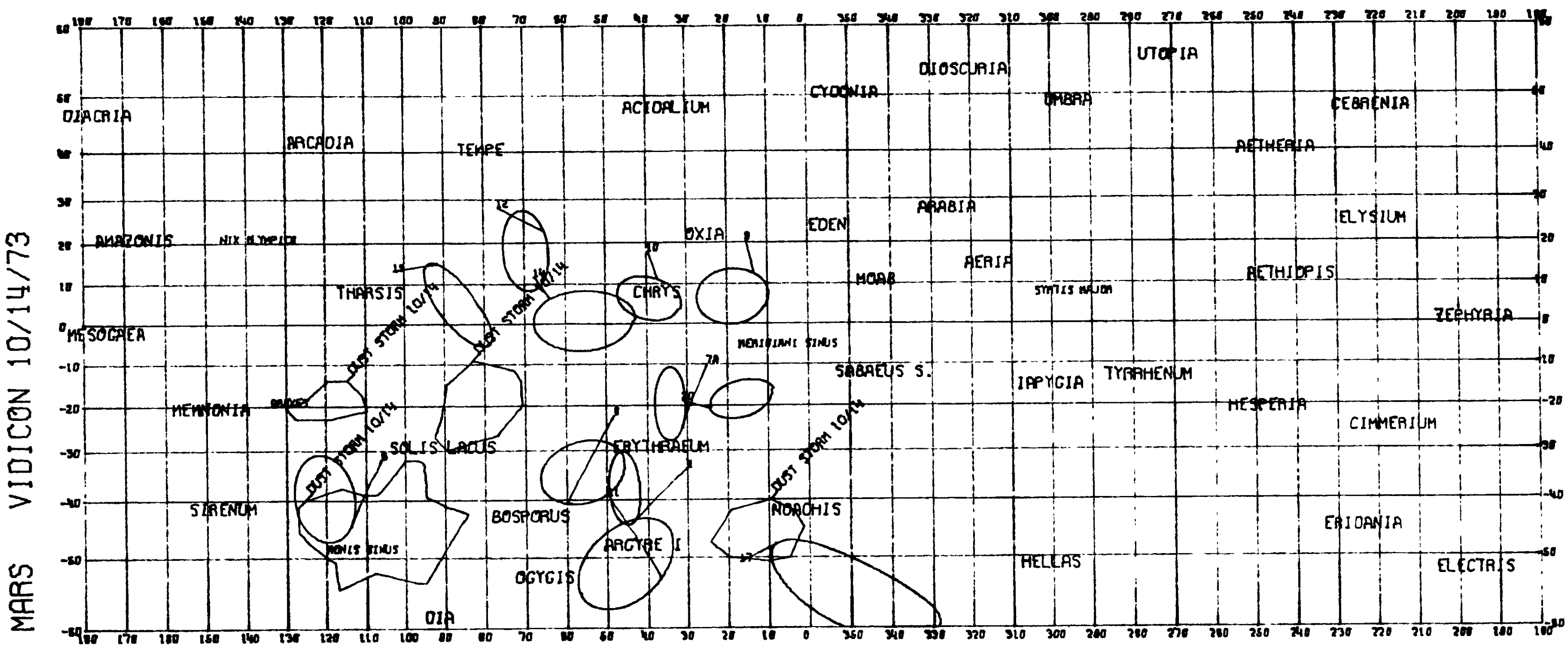

Figure 14. Mercator projection of Mars showing elliptical photometer spot boundaries and the dust storm as of October 14, 1973 - the same night that the vidicon images were taken.

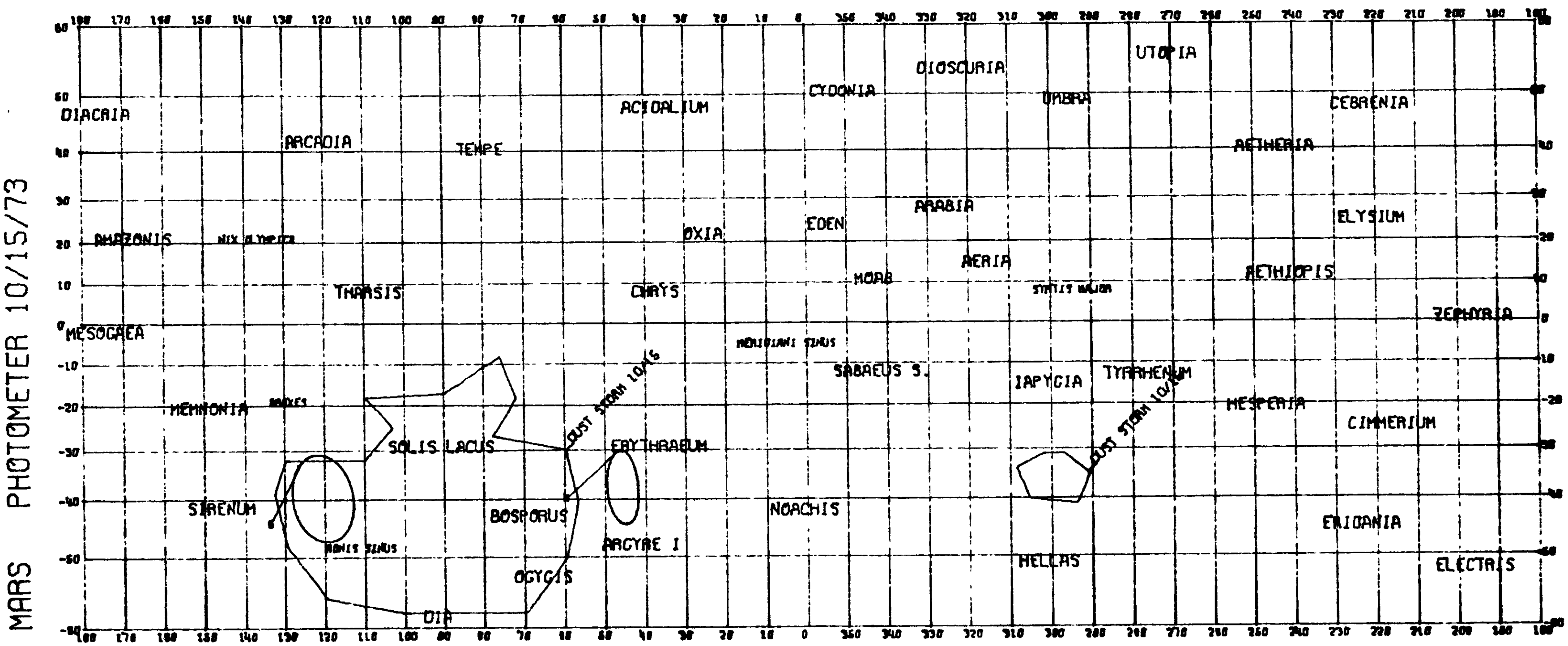

Figure 15. Mars map with the dust storm as of October 15, 1973 and two of the photometer spots (4 & 6) taken that same night.

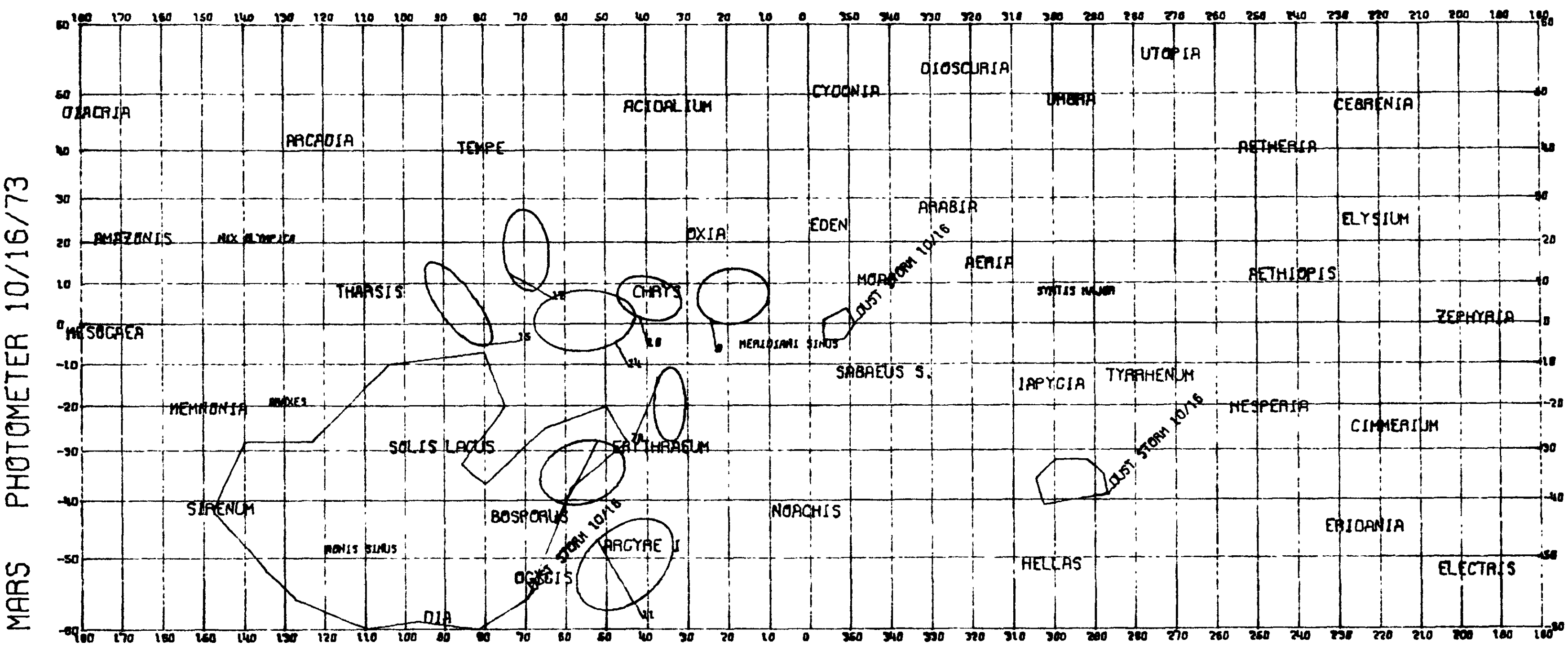

Figure 16. Mars map with the dust storm as of October 16, 1973 and photometer spots 7A through 15 taken that same night.

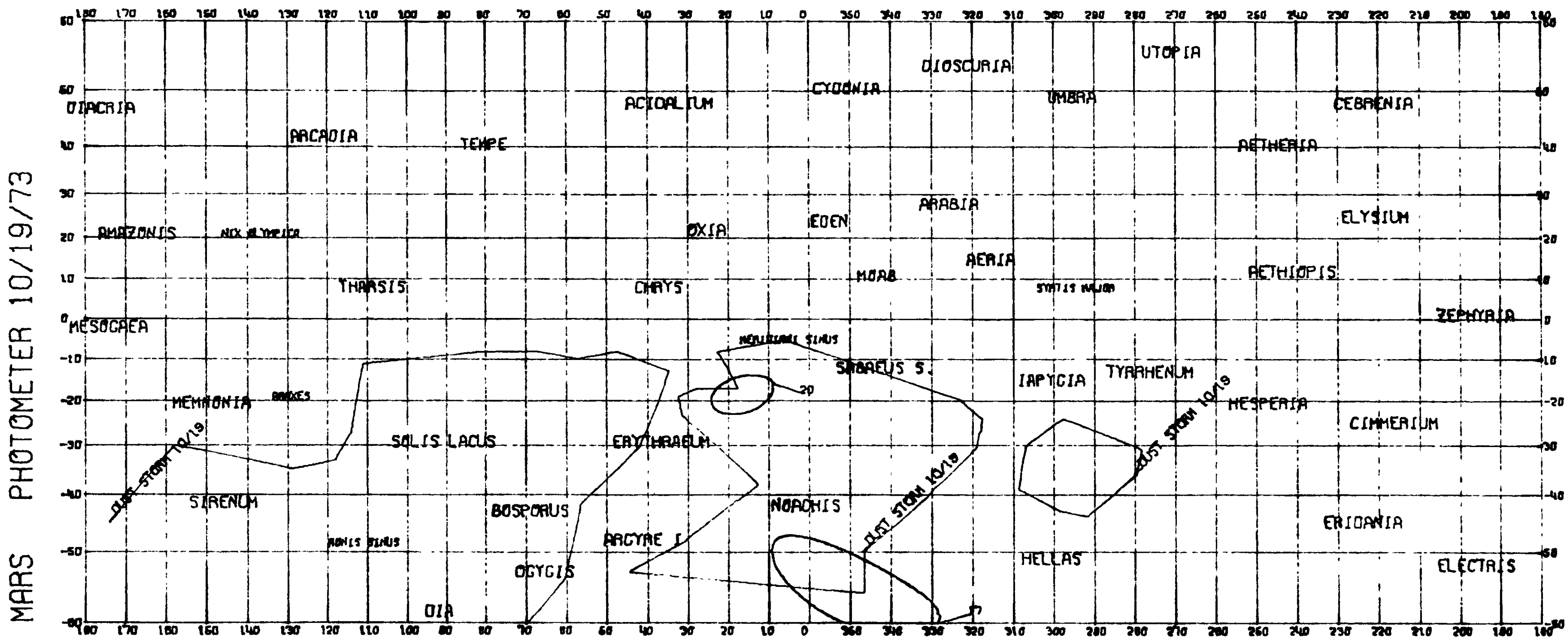

Figure 17. Map of Mars with the dust storm as of October 19, 1973 and photometer spots 17 and 20 taken that same night.

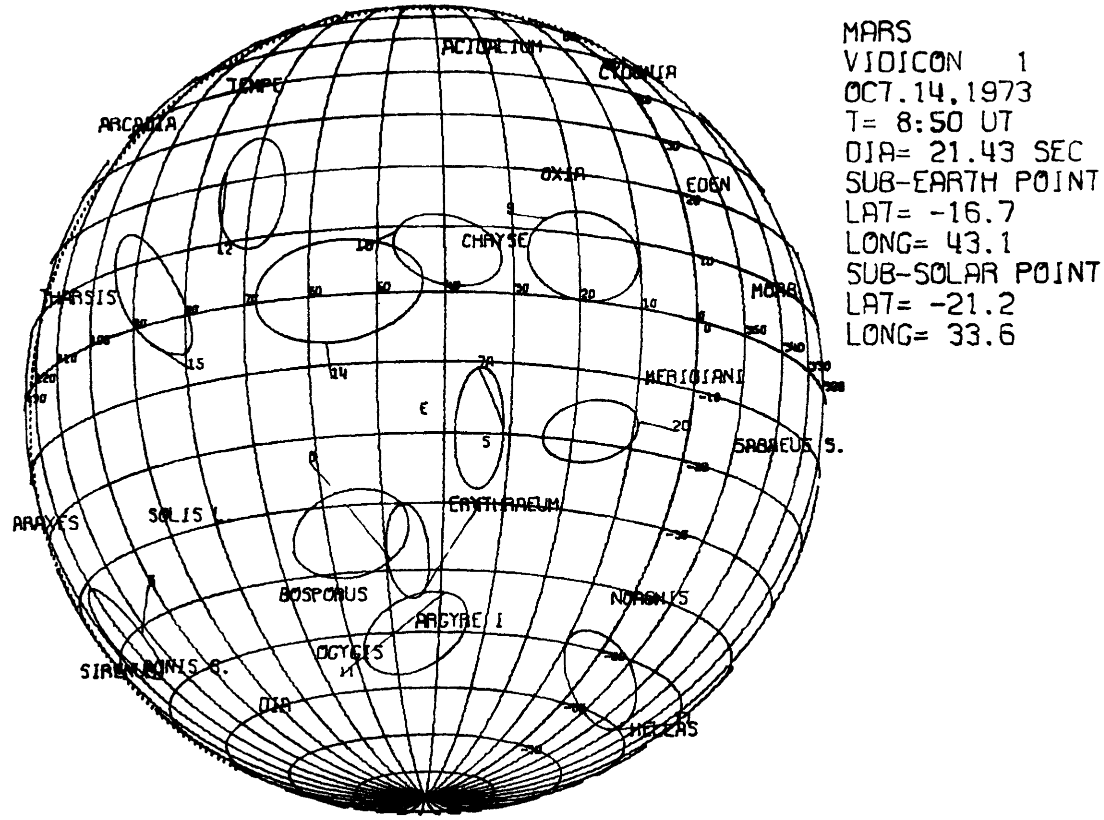

Figure 18. Photometer spots as seen on first and last images.

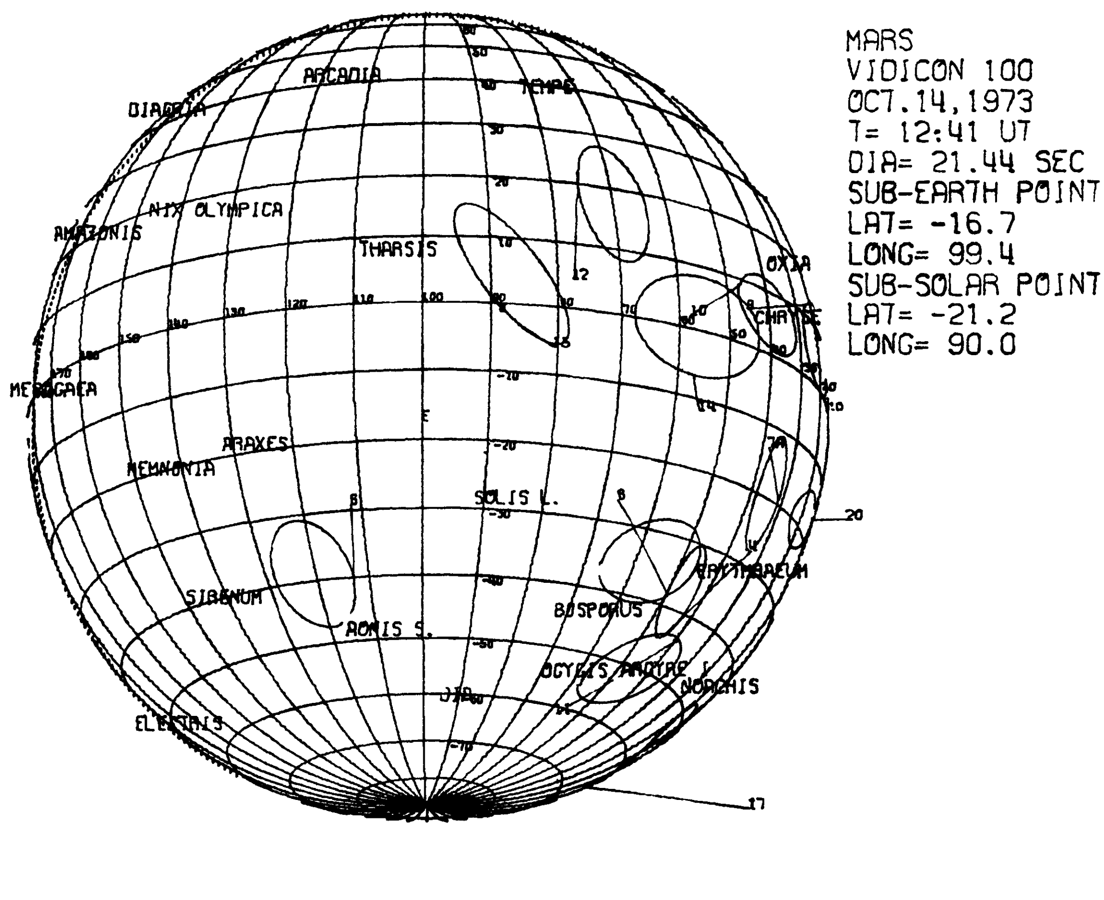

October 14, 1973. Furthermore, to facilitate identifying these spots on the maps, a list of the latitude and longitude center coordinates of the spots can be found in Table 1. For all of these spots relative reflectance spectra have been produced from the photometer data using reduction routines similar to those found in the image processing system - DIPSYS. By carrying out the image processing described in the last section, relative reflectance spectra for the same spots on Mars have been extracted from the calibrated vidicon images. A comparison between these two sets of data follows.

A dark region on Mars appears 'dark' because of a broad absorption band in the near infrared which is an attribute of Fe^{2+} minerals in the soil (Adams and McCord, 1969; R.L. Huguenin, J.B.Adams, and T.B.McCord, manuscripts in preparation, 1974). Bright areas are 'bright' because they lack this broad absorption feature. A relative reflectance spectra for a bright area divided by a dark area will therefore produce a curve rising above 1.0 in the near infrared. If the opposite case is taken (dark divided by bright), the curve will fall below 1.0 in the near infrared.

According to the log book kept during the photometer observation period, as well as by visual and graphical interpretation of the data, photometer Spot 8 (34°S, 56°W) was the darkest of all the photometer spots. However, Spot 20 (18°S,

Spot	Latitude	Longitude
4	38°S	46°W
6	39°S	121°W
7A	20°S	34°W
8	34°S	56°W
9	7°N	19°W
10	6°N	39°W
11	51°S	46°W
12	18°N	69°W
14	1°N	55°W
15	5°N	87°W
17	55°S	351°W
20	18°S	16°W

Table 1. A list of the photometer spot center coordinates.

16°W) was the darkest of all the spots reduced from the vidicon image data. If both spots were equally dark in both cases, then the photometer relative reflectance curve of Spot 8 divided by Spot 20 (Spot 8/Spot 20) would be a straight line. So also would be the vidicon derived relative reflectance curve of Spot 8/Spot 20. Both of these plots should then overlay as a single straight line equal to 1.0 at all wavelengths. Figure 19 shows the relative reflectance of Spot 8 divided by Spot 20 as reduced from both the photometer data and the vidicon data. The 'v's represent vidicon data and the 'p's represent photometer data. Clearly the reflectance curves for these ratioed spots are neither flat at 1.0 nor even similar. This example highlights the interpretation problems imposed by the expanding dust storm.

In Figure 19 the vidicon data implies that Spot 8 was brighter than Spot 20. Yet the photometer data implies that Spot 8 was darker than Spot 20. Either Spot 8 became darker between October 14 and October 16 or Spot 20 became brighter by October 19, or both. The fact that significant albedo changes did occure between the observations of each of these spots is outlined by the growth of the dust storm as shown in Figures 14, 16 and 17. For the vidicon data, Spot 20 (in the dark region - Mare Erythraeum) was far removed from any dust clouds, as was Spot 8. Apparently Spot 20 material is intrin-

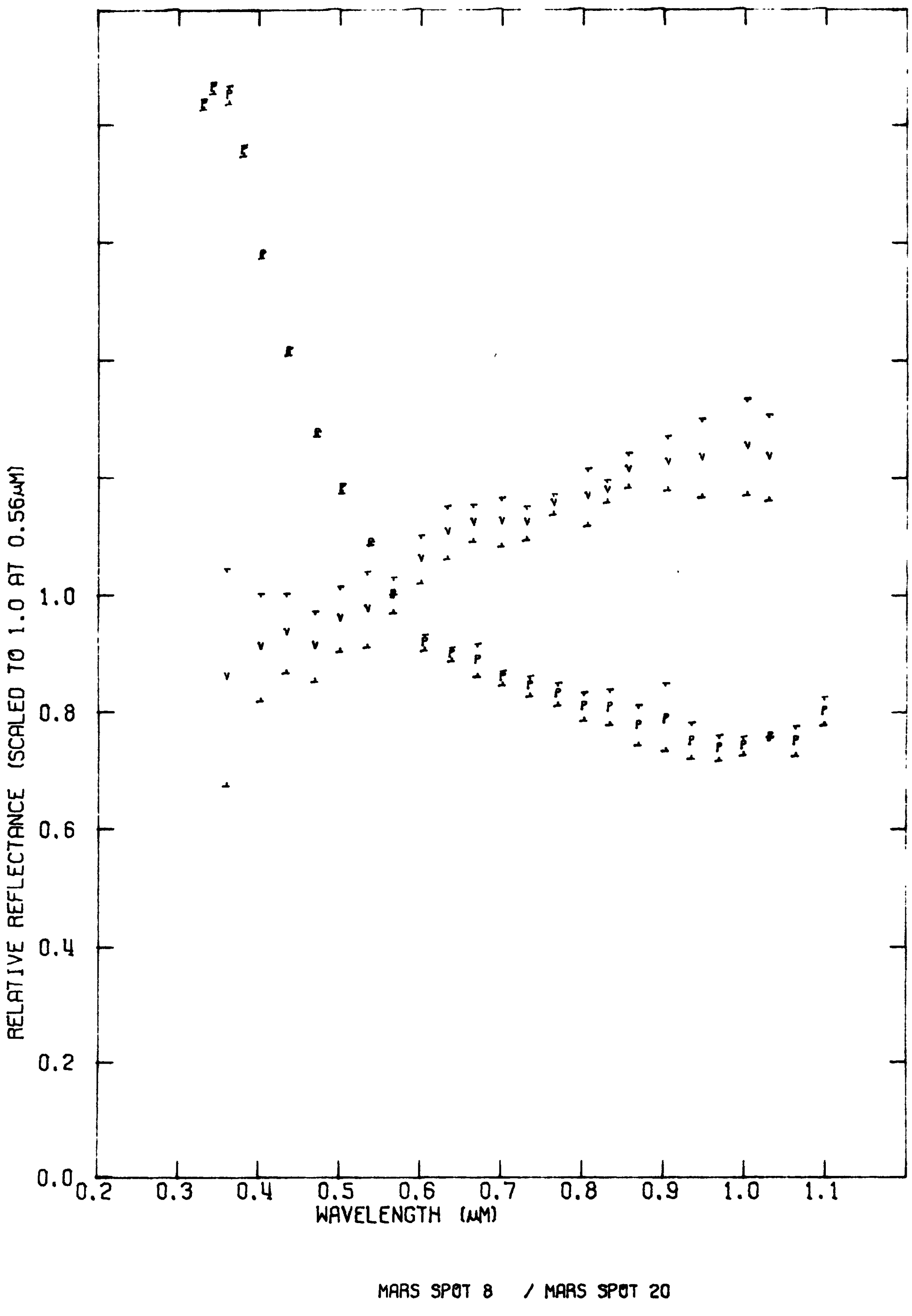

RELATIVE REFLECTANCE (SCALED TO 1.0 AT 0.56µM)
0.0
0.2
0.4
0.6
0.8
1.0
0.2
0.3
0.4
0.5
0.6
0.7
0.8
0.9
1.0
1.1
WAVELENGTH (µM)
MARS SPOT 8 / MARS SPOT 20

Figure 19

sically darker than Spot 8 material, leading to the rising vidicon curve in Figure 19. But by October 19, Spot 20 was almost totally engulfed by bright dust. Spot 8 in the photometer data (Figure 16) overlays part of the dust storm but it apparently recorded enough of the dark Erythraeum material to ultimately make it darker relative to Spot 20. Hence the falling photometer curve in Figure 19.

To remove as much of the adverse effects of the growing dust storm as possible, a search was made for spots that were far removed from the dust storm in both the photometer and vidicon image data. As Figures 14 and 16 reveal, Spot 9 (7°N, 19°W) and Spot 10 (6°N, 39°W) both fit this criteria.

Figure 20 shows the overlay of photometer and vidicon data for the relative reflectances of Spot 10/Spot9. Within the error bars the two curves match, indicating that the vidicon system does indeed return valid photometric data. As a result, Spot 9 was chosen as the denominator for all relative reflectance spectra. Spot 10 was not chosen since as the map in Figure 16 indicates, Spot 10 is closer to the dust cloud. Discrepancies between photometer and vidicon data must, therefore, be interpreted in light of (1) the rapid albedo changes on Mars during the dust storm - as the discussion of Spot 8/Spot 20 has revealed - and (2) possible inaccuracies in the Spot-Mapping program.

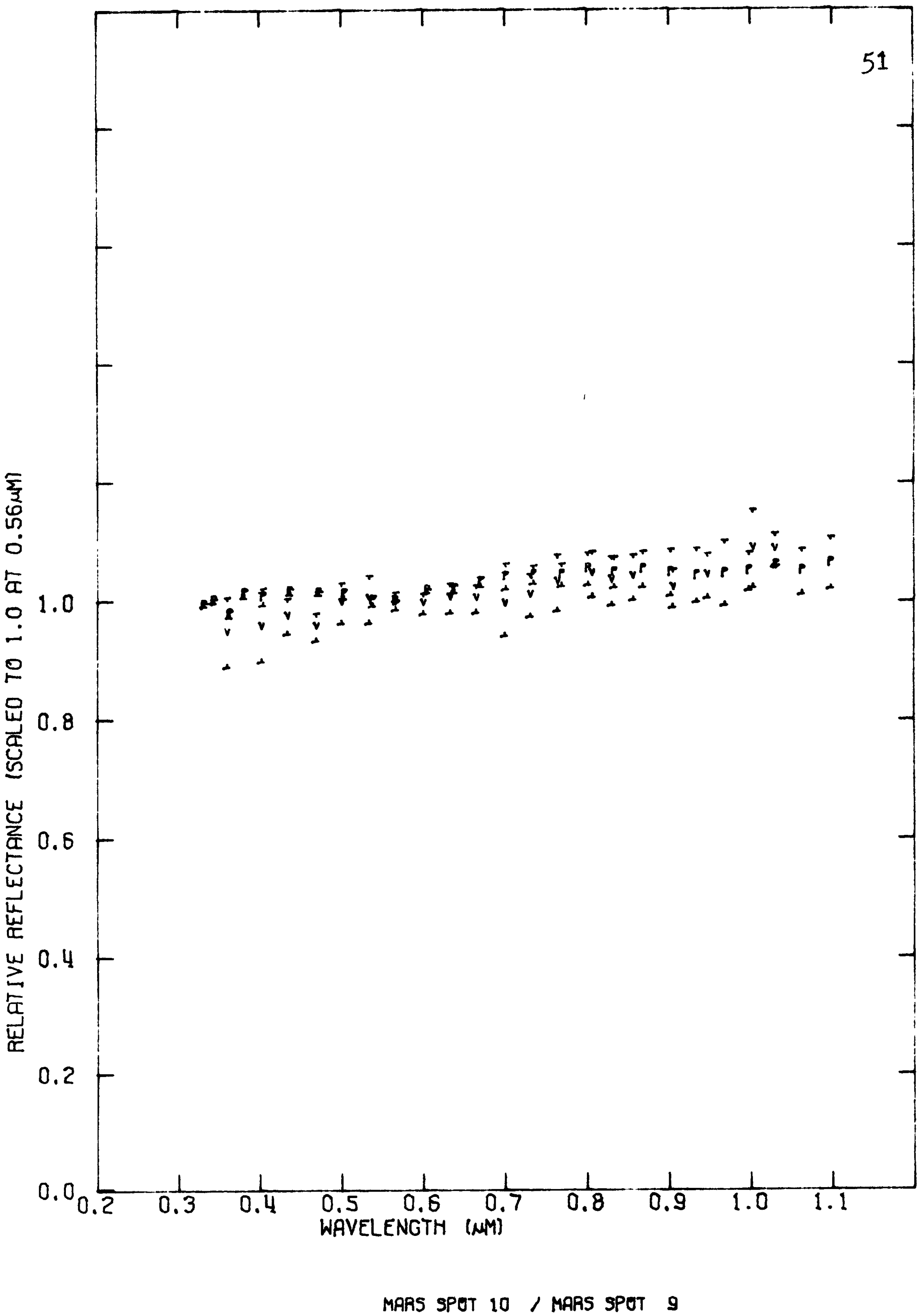
RELATIVE REFLECTANCE (SCALED TO 1.0 AT 0.56μM)
1.0
0.8
0.6
0.4
0.2
0.0
0.2
0.3
0.4
0.5
0.6
0.7
0.8
0.9
1.0
1.1
WAVELENGTH (μM)
MARS SPOT 10 / MARS SPOT 9

Figure 20

Spot 4 (38°S, 46°W) also lies over the dark Erythraeum region. Ratioed to a bright area, which Spot 9 is, Spot 4 should produce a curve that decreases in the near infrared. Figure 21 shows the relative reflectance spectra for Spot 4/ Spot 9. In general the photometer data is in agreement with this prediction. The vidicon data is not. For both sets of data Spot 4 is removed from the dust storm, especially in the vidicon data. However, as the analysis in Section III has shown, the furthest, albeit tenuous, extent of the dust storm is best revealed in the blue. The scatter in the vidicon data for Spot 4/Spot 9, particularly in the blue, may be caused by the thin clouds reaching down from the Coprates Canyon area (see Figure 4).

Spot 6 (39°S, 121°W) captures the dust storm in both sets of data. Figure 22 shows the relative reflectance of Spot 6/Spot 9. Again there is great scatter in the vidicon data, especially in the blue. Spot 6 lies over the Aonis Sinus cloud, of which the extreme albedo variations in the blue have already been discussed. This accounts for the wide error bars around 0.40 microns. In the photometer data Spot 6 is brighter than Spot 9 as would be expected of a dust storm composed of a concentration of bright area material. Overlooking the data scatter in the vidicon derived curve, the spectra is contrary to the expected trend. Perhaps the

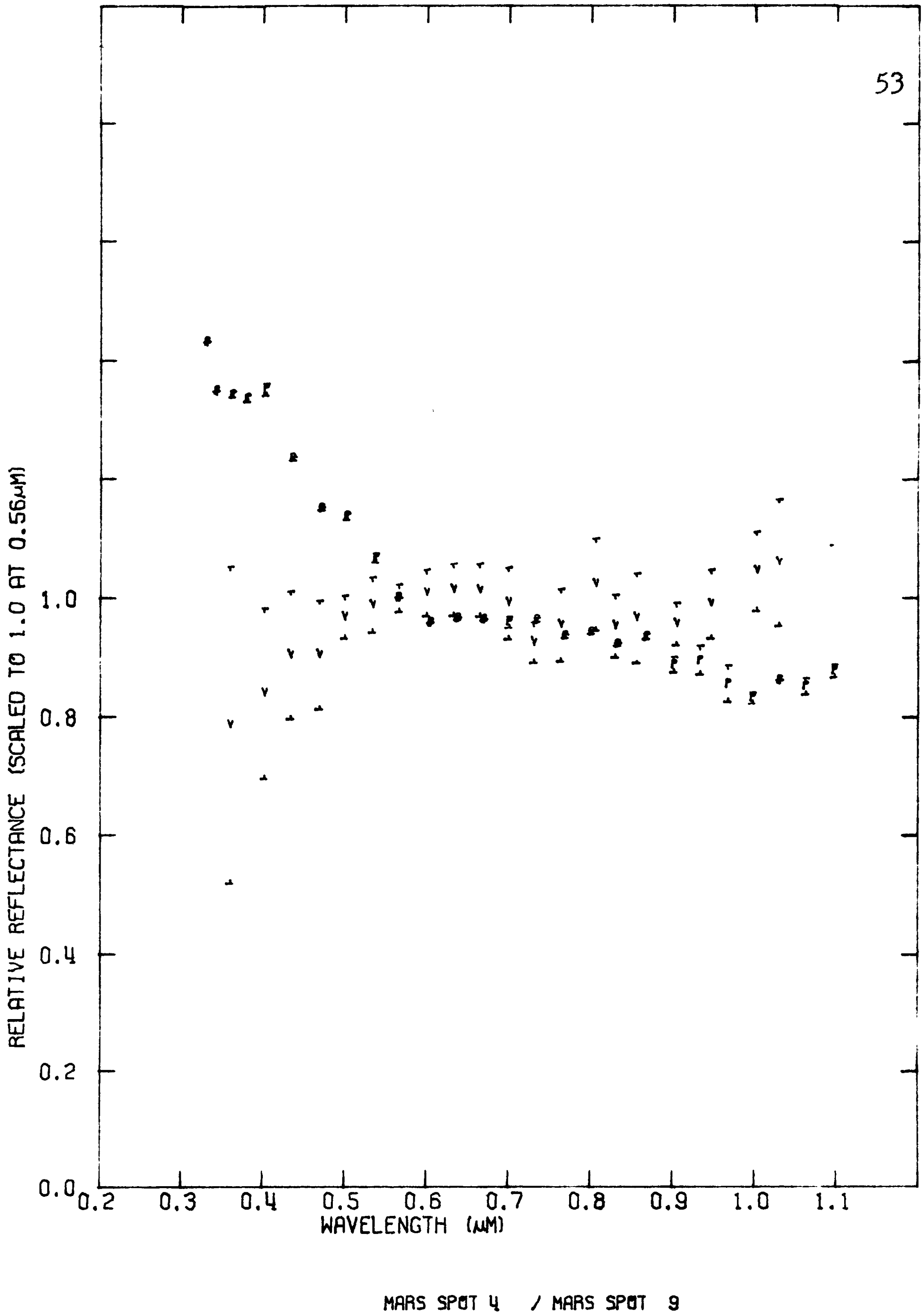
RELATIVE REFLECTANCE (SCALED TO 1.0 AT 0.56μM)
1.0
0.8
0.6
0.4
0.2
0.0
0.2 0.3 0.4 0.5 0.6 0.7 0.8 0.9 1.0 1.1
WAVELENGTH (μM)
MARS SPOT 4 / MARS SPOT 9

Figure 21

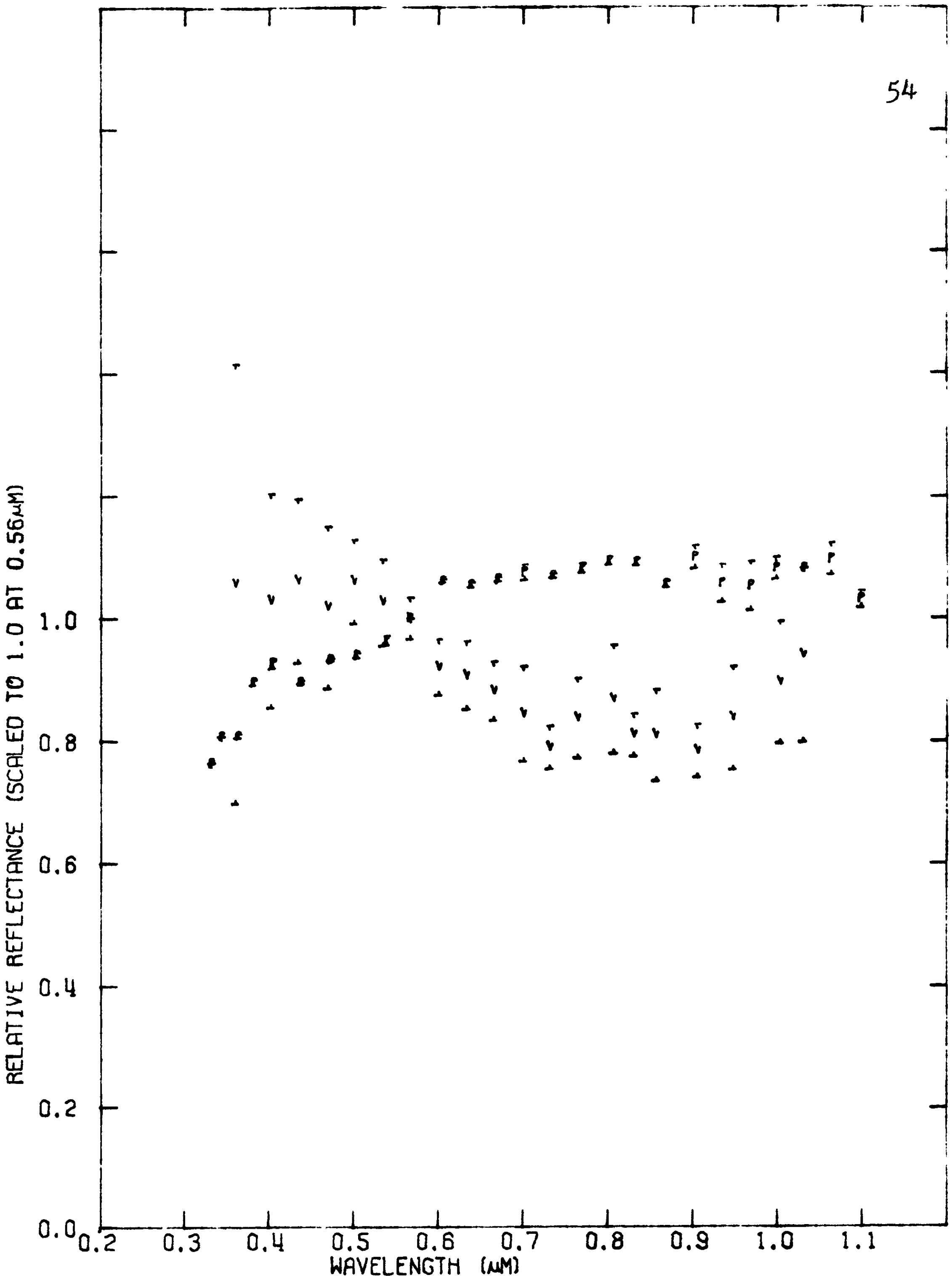

MARS SPOT 6 / MARS SPOT 9

Figure 22

darkening of Spot 6 relative to Spot 9 in the 0.65 micron region is caused by the elliptical spot boundary only partially overlaying the apparently tenuous Aonis Sinus cloud and encompassing some of the dark gap between this cloud and the region west of the Solis Lacus cloud (see Figure 4).

Inaccuracies caused by the image processing (using the Center-Seeking and Spot-Mapping programs) may have caused some of the dissimilarities discussed so far. But Spot 10/ Spot 9 in Figure 20 does not bear this out. However, Spot 10 and Spot 9 are in close proximity, and both are bright areas. Inaccuracies in the image processing cannot necessarily be expected to be revealed by the ratio of Spot 10/Spot9. However, Spot 7A does clearly demonstrate the precision of the image processing.

Spot 7A (20°S, 34°W) lies in the heart of the Erythraeum dark region. It is out of the main body of the dust storm in both sets of data. Spot 7A is also distant from Spot 9 as Figure 18 in particular points out. Figure 23 displays the relative reflectance of Spot 7A/Spot 9 for the photometer and vidicon data. The drop below 1.0 in the red end of the spectrum indicates that Spot 7A is indeed darker than Spot 9. The curves match very well - revealing the accuracy of the image reductions. The photometer curve rise around 0.90 microns may be caused by a slight dustiness from the nearby

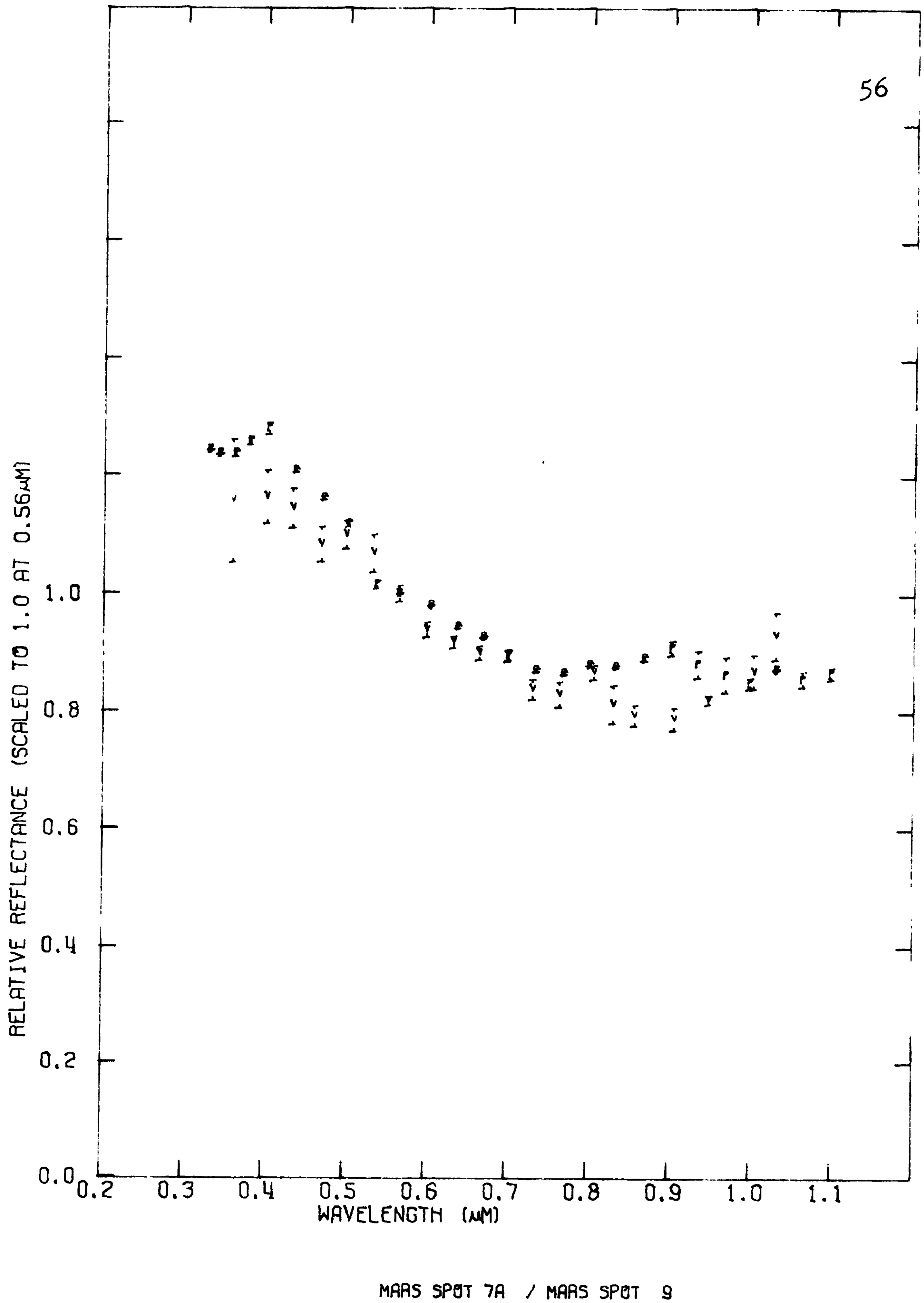
RELATIVE REFLECTANCE (SCALED TO 1.0 AT 0.56µM)
0.0
0.2
0.4
0.6
0.8
1.0
0.2
0.3
0.4
0.5
0.6
0.7
0.8
0.9
1.0
1.1
WAVELENGTH (µM)
MARS SPOT 7A / MARS SPOT 9

Figure 23

dust cloud (see Figure 16). The large error bars around 0.35 microns in the vidicon data may again be due to the blue haze northeast of Solis Lacus (see Figure 4).

Spot 11 (51°S, 46°W) in Figure 24 shows dissimilarities between vidicon and photometer data around 0.73 microns and 0.90 microns. These two features may have been washed out of the photometer curve by the reddening caused by dust from the nearby storm (Figure 16). It should be kept in mind that the boundaries of dust clouds are certainly not as accurate as the straight lines in Figures 14 to 17 might indicate.

Spots 12, 14 and 15 (18°N,69°W, 1°N, 55°W and 5°N, 87°W, respectively) in Figures 25, 26 and 27 all show the same basic trend in the vidicon data, namely an apparent rise in the near infrared. The scatter in this vidicon data is, however, severe and may be attributed to albedo variations in the length of clouds north of Solis Lacus in the region of the Coprates Canyon, as well as in the cloud over Tharsis. Another cause of the data scatter that is more fundamental to the image processing done to the vidicon data may also be playing a part here. The Spot-Mapping program averages all intensity values falling within a given ellipse. In simulating photometer data, the program is therefore assuming that the photometer aperture covered the entire area within the ellipse. This is not true. In fact, to within 90% confidence, the

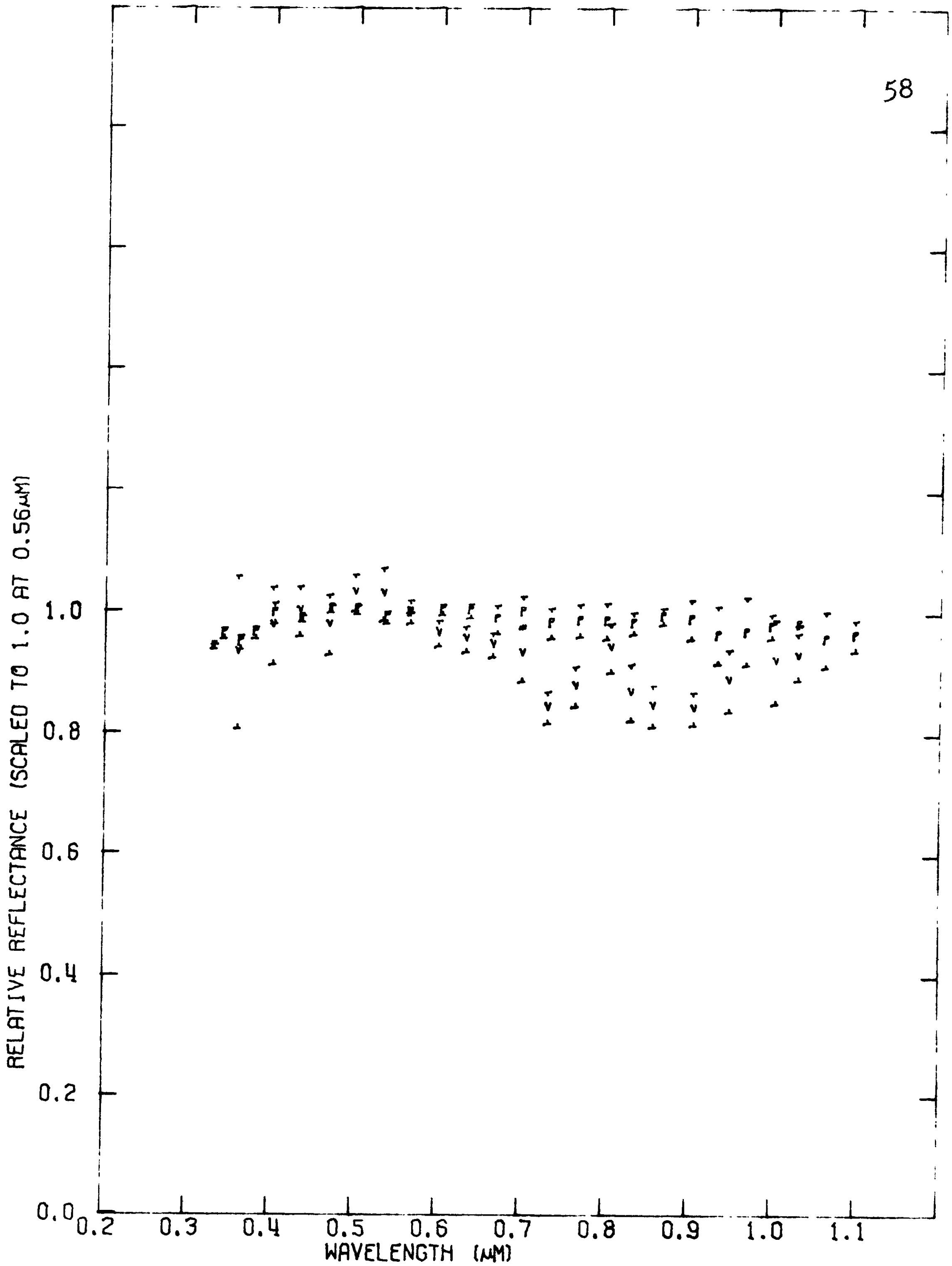

MARS SPOT 11 / MARS SPOT 9

Figure 24

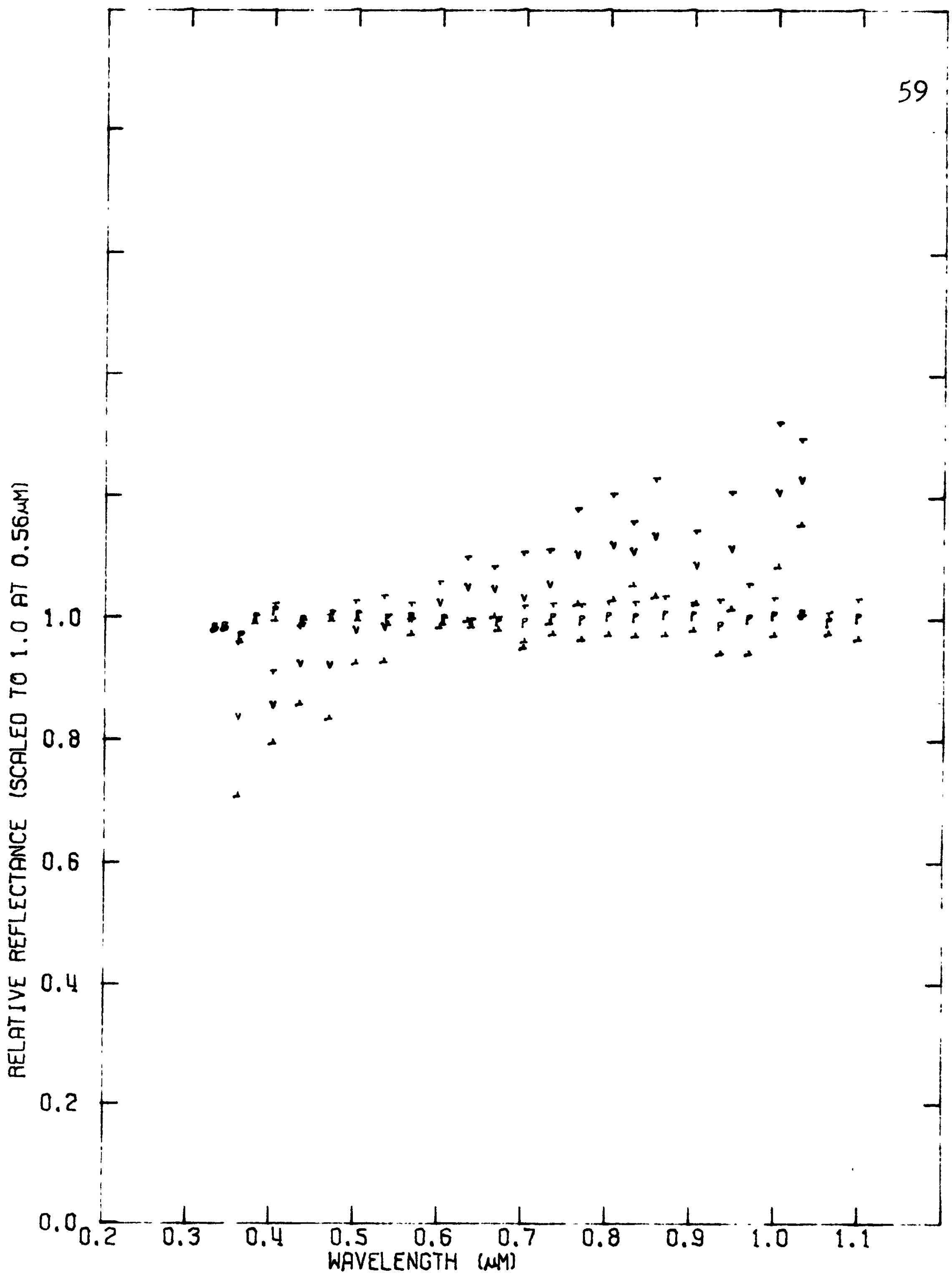

MARS SPOT 12 / MARS SPOT 9

Figure 25

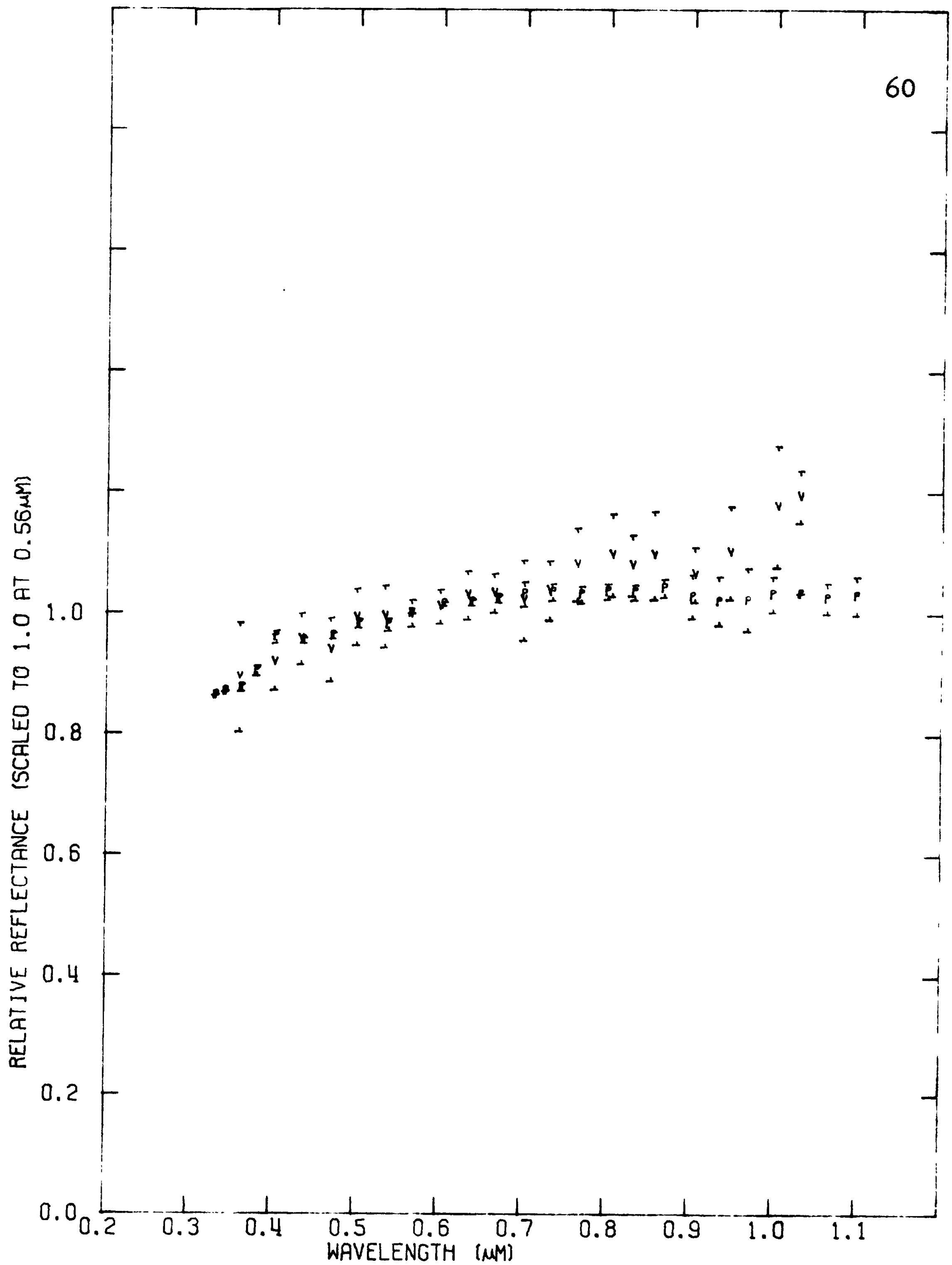

MARS SPOT 14 / MARS SPOT 9

Figure 26

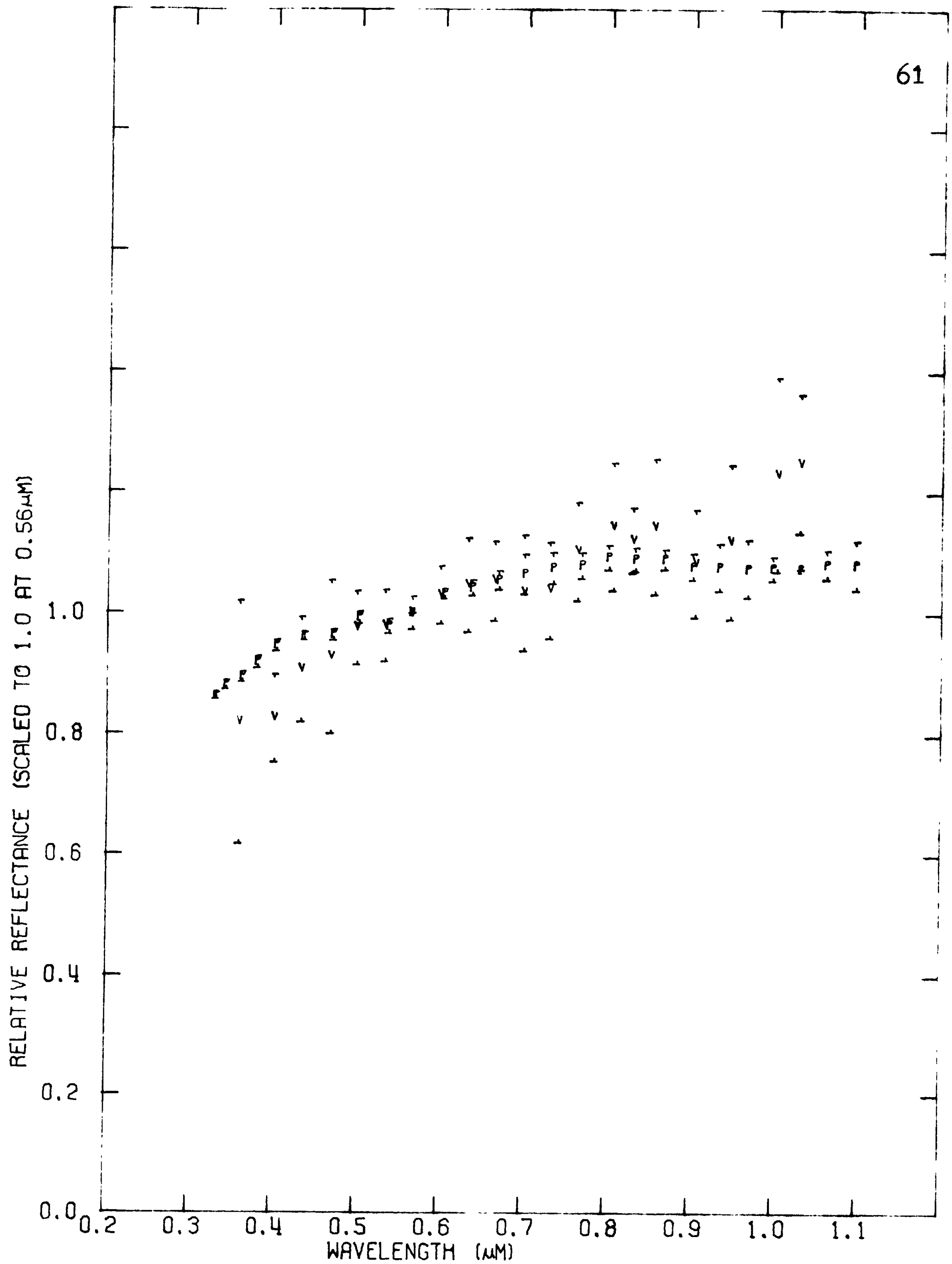

MARS SPOT 15 / MARS SPOT 9

Figure 27

photometer aperture only wandered around somewhere within the ellipse. Spots 12, 14 and 15 lie over and near regions of rapidly changing albedo. The Tharsis and Coprates clouds, tenuous as they appear to be on October 14, may have been different or may not have existed at all when the three photometer spots were measured on October 16. This design weakness in the Spot-Mapping program may also be responsible for the dissimilarities seen in Spot 11/Spot 9, Figure 24.

Another weakness in the vidicon data is highlighted by the scatter in Figure 28. This shows the relative reflectance of Spot 17/Spot 9. Figure 17 shows that the dust storm lies partly in photometer Spot 17. The rest of Spot 17 covers the dark area of southern Noachis. Apparently the photometer aperture recorded mostly the dark area reflected light since Spot 17 is darker than Spot 9 in the photometer curve of Figure 28. The vidicon curve follows this trend but with severe scatter. As can be seen in Figure 18, Spot 17 lies near the east limb of Mars for the first image and most of the spot eventually passes over the horizon. The scatter in the data results from difficulties the Spot-Mapping program has in locating a spot near the limb of the planet. The mean radius returned by the Center-Seeking program may prevent the Spot-Mapping program from aquiring limb data or it may cause the Spot-Mapping program to overreach the limb and return false

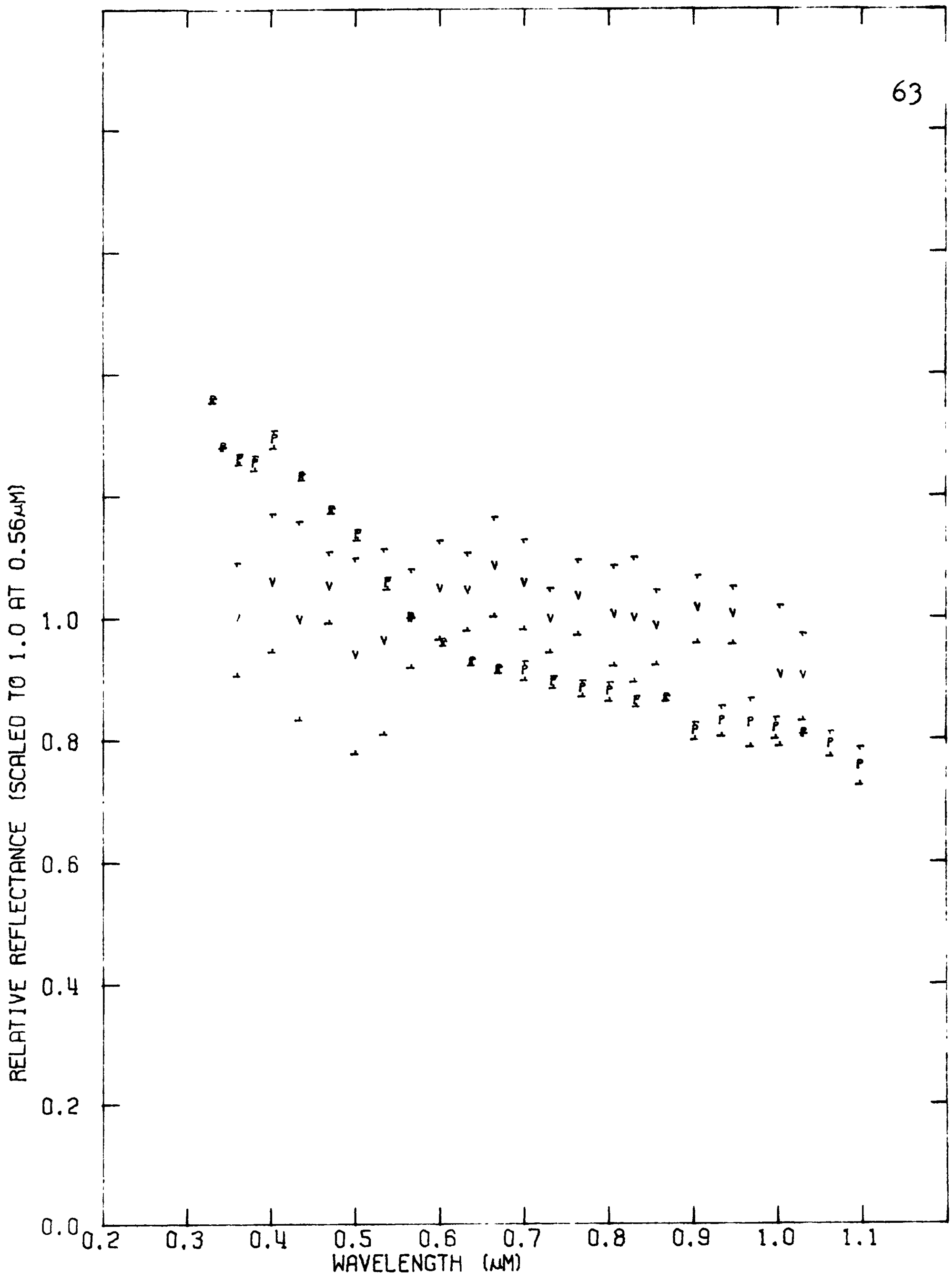

MARS SPOT 17 / MARS SPOT 9

Figure 28

data from intensity values beyond the planet. Data extracted from any spot near the limb is suspect. This problem has probably contributed to the vidicon data scatter not only in Spot 17, but also in Spot 15, Spot 6 and Spot 9 (the denominator!).

Finally, just to conclude with a clear cut example, Figure 29 shows the relative reflectance spectra for Spot 20/ Spot 9. In the vidicon data the curve indicates that Spot 20 is darker than Spot 9 as it should since both spots are out of the dust storm (Figure 14) and Spot 20 overlays the dark Mare Erythraeum whereas Spot 9 overlays the bright area of eastern Chryse. In the photometer data Spot 20 appears brighter than Spot 9, primarily because photometer Spot 20 was measured on October 19 when the dust storm covered most of Mare Erythraeum, including most of Spot 20 (Figure 17).

Since the vidicon tube has a demonstrated photometric responce, the final step in the reduction of the vidicon data, which is the production of reflectance spectra normalized to the Sun, could directly use the photometer data. Multiplying all the vidicon spectral reflectivities relative to Spot 9 by the ratio of Spot 9/Sun - as derived from the photometer data using standard stars - will yield reflection spectra normalized to the Sun for any area on the visible face of Mars. An interpretation of the vidicon data could

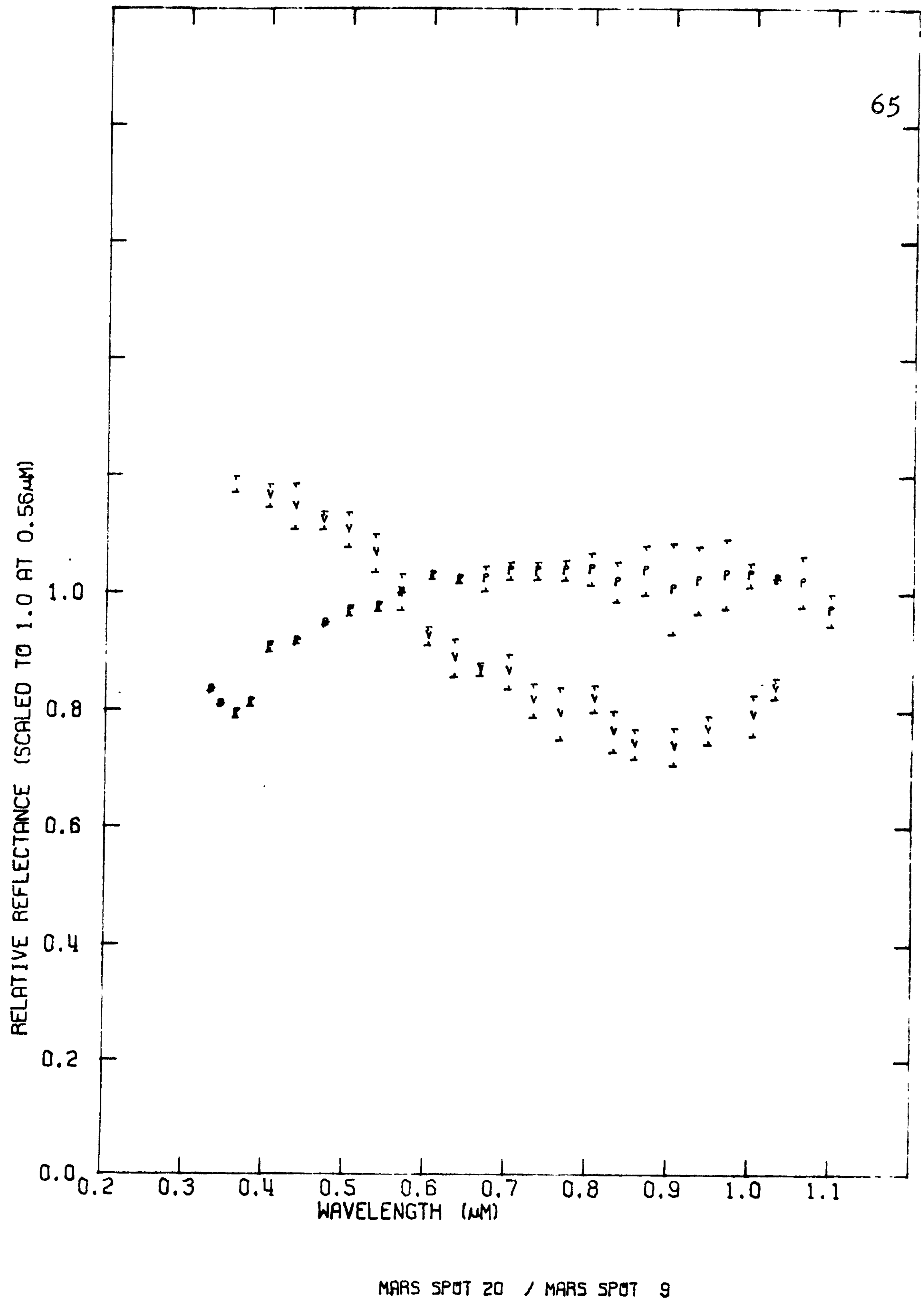
RELATIVE REFLECTANCE (SCALED TO 1.0 AT 0.56μM)
1.0
0.8
0.6
0.4
0.2
0.0
0.2
0.3
0.4
0.5
0.6
0.7
0.8
0.9
1.0
1.1
WAVELENGTH (μM)
MARS SPOT 20 / MARS SPOT 9

Figure 29

then begin without the ambiguities and subtleties of relative reflectance spectra. This final step awaits only an accurate determination of Spot 9/Sun - currently in the works.

As the data presented in this section reveals, the Vidicon Imaging System coupled with the image processing system returns accurate, two-dimensional photometric data. The discrepancies between the vidicon image data and the photometer data of October, 1973 can mostly be attributed to the obscuring caused by the expanding dust storm. Also, the error bars in the vidicon data are in general greater than the photometer error bars. This is probably caused by either (1) insufficient data (100 images exposed through 20 filters gives only five complete sets of vidicon data) or (2) small inaccuracies in finding the spots from image to image by the Spot-Mapping program. However, a few selected cases (Figures 20, 23 and 29 for example) clearly exhibit the power of this data collection system. It is now possible, given the vidicon system, to specify any area on Mars and produce a reflection spectra for that area.

VI. Concluding Remarks

The observations of Mars made with the Vidicon Imaging System during the October, 1973 opposition have produced a fund of valuable information. The 1973 dust storm was imaged in its early developmental stages. The diurnal evolution of the dust clouds has been captured in explicit detail. The rapid albedo variations in these clouds can successfully be explained by condensed and adsorbed volatiles adhering to the dust grains during the Martian night and then sublimating following exposure to sunlight. The dust clouds themselves are seen undergoing rapid alterations in structure. The digital format of the vidicon images facilitates data reductions. The images can be artificially rotated to view interesting features from different angles. The intensity values which make up the images are themselves individual photometric sensors. The reduction of the images to spectral reflectivity curves has been described, emphasizing the power of the vidicon tube to provide two-dimensional, narrow-band photometry. Unfortunately, the presence of the dust storm has a detrimental obscuring effect on spectral reflectivity data which prevents a detailed compositional study of the Martian surface. Perhaps during the next opposition Mars will present itself with an atmosphere unobscured by dust. If so, the full disk photometric coverage of the planet provided by the Vidicon Imaging System will yield spectral reflectivity data for all resolvable areas on the visible face.

The Vidicon Imaging System coupled with the DIPSYS image processing system - including especially the programs described in this thesis - has a usefulness other places than just Mars. Elsewhere in the Solar System there are intriguing curiosities, such as the UV clouds on Venus, transient events on Jupiter, assorted moons with assorted surfaces, and the several rings of Saturn - to name a few. Undoubtedly the Vidicon Imaging System will be applied to these fascinating objects with the same success displayed during the October, 1973 Mars observations.

REFERENCES

Abramenko,A.N. and V.V.Prokof'eva (1975) "Television Observations of Martian Cloud Formations in 1973: Preliminary Results," Icarus 24, p.379-382.

Adams,J.B. and T.B.McCord (1969) "Mars: Interpretation of Spectral Reflectivity of Light and Dark Regions," JGR 74, p.4851-4856.

Baum,W.A. (1974) "Earth-Based Observations of Martian Albedo Changes," Icarus 22, p.363-370.

Capen,C.F. (1973) I.A.U. Circular 2587, Smithsonian Astrophys Obs.

Carr,M.H.,H.Masursky, and R.S.Saunders (1973) "A Generalized Geologic Map of Mars," JGR 78, p.4031.

Dollfus,A. (1961) "Polarization Studies of Planets," Chapter 9 in Planets and Satellites, edited by G.P.Kuiper and B.M. Middlehurst, (Chicago: University of Chicago Press).

Gierasch,P.J. and R.M.Goody (1973) "A Model of a Martian Great Dust Storm," J.Atmos.Sci. 30, p.169-179.

Huguenin,R.L. (1974) "The Formation of Goethite and Hydrated Clay Minerals on Mars," JGR 79, p.3895-3905.

Huguenin,R.L. (1975) private communication.

Leovy,C.B.,G.A.Briggs,A.T.Young,B.A.Smith,J.B.Pollack,E.N. Shipley, and R.L.Wildey (1972) "The Martian Atmosphere: Mariner 9 Television Experiment Progress Report," Icarus 17, p.373-393.

Leovy,C.B.,R.W.Zurek, and J.B.Pollack (1973) "Mechanisms for Mars Dust Storms," J.Atmos.Sci. 30, p.749-762.

Martin,L.J. (1974) "The Major Martian Dust Storms of 1971 and 1973," Icarus 23, p.108-115

McCord,T.B. and J.Bosel (1973) "Silicon Vidicon Astronomy at MIT," presented at the symposium, "Astronomical Observations with Television-Type Sensors," held May 15-17, 1973, at the University of British Columbia.

McCord,T.B.,C.Pieters and M.Fierberg (1975) paper in draft.

McCord,T.B. and J.A.Westphal (1971) "Mars: Narrow-Band Photometry, from 0.3 to 2.5 Microns, of Surface Regions During the 1969 Apparition," Astrophys.J. 168, p.141-153.

McCord,T.B. and J.A.Westphal (1972) "Two-Dimensional Silicon Vidicon Astronomical Photometer," Applied Optics 11, p.522-526.

Mink,D.J. (1974) "Determination of Martian Surface Reflectivity from 0.4 to 1.1 Microns Using a Vidicon Spectrometer," M.S. Thesis, M.I.T., June 1974.

Pieters,C. and T.B.McCord (1974) "Two Dimensional Vidicon Spectral Images: Information on the Composition and Evolution of Mare Humorum," Am.Astro.Soc.Bulletin 6, p.374.

Sagan,C.,J.P.Phaneuf and M.Ihnat (1965) "Total Reflection Spectrophotometry and Thermogravimetric Analysis of Simulated Martian Surface Materials," Icarus 4,p.43-61.

Smith,S.A. and B.A.S.Smith (1972) "Diurnal and Seasonal Behavior of Discrete White Clouds on Mars," Icarus 16, p.509-521.